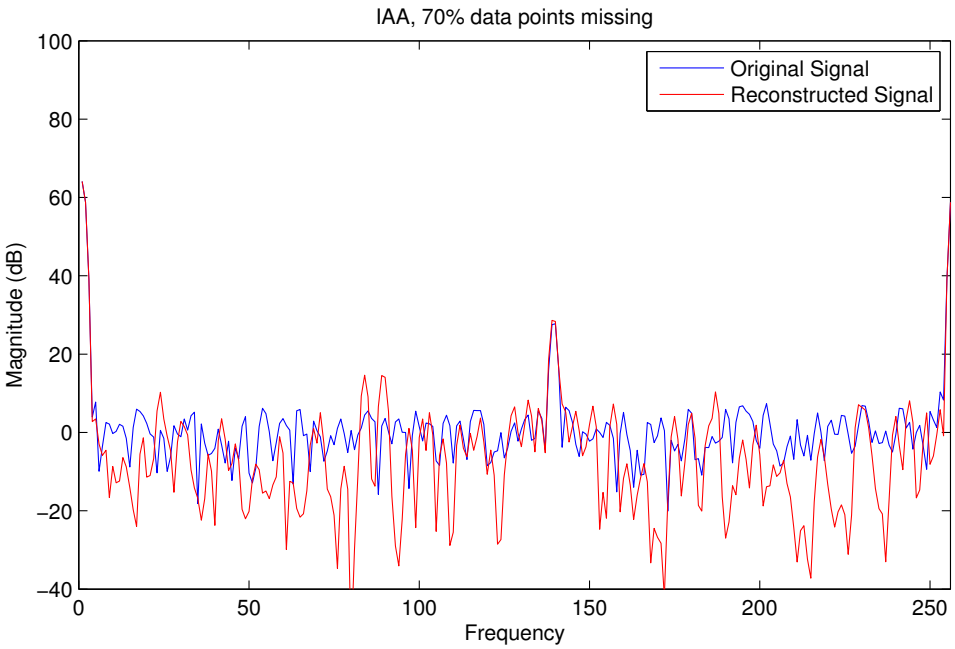

Spectrum Estimation from Incomplete Data

A Study of Methods Suitable for Reducing the Effect of Interference in Medium PRF Radar Data

Johan Rasmusson
Dennis Sångberg

Department of Electrical Engineering
CHALMERS UNIVERSITY OF TECHNOLOGY
Gothenburg, Sweden 2017

Master's Thesis EX044/2017

Spectrum Estimation from Incomplete Data

A Study of Methods Suitable for Reducing the Effect of Interference in Medium PRF Radar Data

Johan Rasmusson
Dennis Sångberg

CHALMERS
UNIVERSITY OF TECHNOLOGY

Department of Electrical Engineering
Chalmers University of Technology
Gothenburg, Sweden 2017

Spectrum Estimation from Incomplete Data
A Study of Methods Suitable for Reducing the Effect of Interference in Medium PRF Radar Data
Johan Rasmusson, Dennis Sångberg

© Johan Rasmusson, Dennis Sångberg, 2017.

Supervisors: Albert Nummelin, Miriam Fransson, SAAB
Examiner: Tomas McKelvey, Electrical Engineering

Master's Thesis EX044/2017
Department of Electrical Engineering
Chalmers University of Technology
SE-412 96 Gothenburg
Telephone +46 31 772 1000

Cover: Reconstruction made by an IAA algorithm from 70% missing data points. Original signal and reconstructed signals are compared.

Typeset in LaTeX
Gothenburg, Sweden 2017

Spectrum Estimation from Incomplete Data
A Study of Methods Suitable for Reducing the Effect of Interference in Medium PRF Radar Data
Johan Rasmusson, Dennis Sångberg
Department of Electrical Engineering
Chalmers University of Technology

Abstract

Airborne radar systems can be disturbed from many kinds of sources. The main different types of disturbances are from interference with other radars/signals or intentional jamming. We will in this thesis examine a way to reduce the effect of the interference by different methods of interpolating over the disturbed data samples. We then reconstruct the frequency spectrum by using missing data algorithms. The missing data algorithms examined are two compressive sensing, which are primal dual and complex approximate message passing and another type of algorithm which is named iterative adaptive approach. To measure the performance we create a signal in which we vary the thermal noise, ground interference and interference from other sources. Each of the algorithms has their own characteristic reconstructed spectrum and our analysis is that the iterative adaptive approach is the most promising for periodic interference with high duty factors where the other algorithms are more vulnerable to ringing which decrease the result of the reconstructed signal. However, CAMP is also interesting due to it being fast and accurate but it struggles when the target is not clear above the noise level.

Keywords: Pulse-Doppler radar, compressive sensing, complex approximate message passing, primal-dual interior point, iterative adaptive approach, spectrum estimation for incomplete data, missing data algorithms.

Acknowledgements

We would like to thank our examiner Tomas McKelvey and our supervisors Albert Nummelin and Miriam Fransson for supporting us and guiding us through our thesis. As well as Åke Andersson for helping and assisting with a lot of technical details and knowledge about radar and signal processing. There were also many others at SAAB who were supportive and gave us advice or recommended us papers that could help us with our work and for that we are very grateful.
Finally, and most importantly we wish to send a special thanks to our families and friends for all encouragement, support and love.

Johan Rasmusson, Dennis Sångberg, Gothenburg, June 2017

Contents

List of Figures

1

Introduction

Already in 1865, James Clerk Maxwell, published *Dynamical Theory of the Electromagnetic Field*, which contains the today famous Maxwell's equations that describe the kinetics of electromagnetic radiation[1].

A radar system uses the electromagnetic spectrum in the radio frequencies and radar technique exists and thrives in a wide variety of fields such as navigation control, remote control, topographic mapping and weather forecasting[2].

The use of radar is becoming more common to detect targets of interest. This results in that the signal one receives to the radar is not necessarily an echo from the signal one emitted but may be that of another radar, which will be much stronger than an echo at the same range. Another problem may be that if one does not want to be detected by a radar, one intentionally interferes with e.g. jamming the radar by sending out a strong signal much stronger than any other signal the radar is expected to receive. Due to this electronic counter measures (ECM) and electronic counter counter measures (ECCM) is a constantly evolving field of work.

In this thesis we will examine a way to reduce the effect of the interference by considering the interfered signals as corrupted and removing them from the incoming data to the radar system. We then reconstruct the frequency spectrum by using missing data algorithms. The missing data algorithms examined are two forms of compressive sensing, which are primal-dual and complex approximate message passing and another type of algorithm which is named iterative adaptive approach. These algorithms use the fact that a signal usually can be presented in a domain in which it is sparse and by examining the given value in this domain an estimation of the missing data samples can be extracted. In this report the sparse domain has been assumed to be the frequency domain and that from a few strong frequencies the signal can be reconstructed in a satisfying way.

To measure the performance we created a synthetic signal in which we could vary the noise, ground interference and interference from other sources and then we measured some key attributes of the recovered signal from the examined algorithms.

Henceforth, we will focus on a specific type of radar named pulse-Doppler radar and more information on how it works is given in the following chapter.

2

Theory

This chapter provides a brief theoretical background to some key concepts in the problem of retrieving a frequency spectrum from an incomplete data set in the time domain of a pulse-Doppler radar, which will ensure that the reader is familiar with the subjects that are investigated in the method and result.

The reviewed topics are: pulse-Doppler radar theory, signal processing and missing data algorithms. We have chosen to use broad names for these sections, however mostly only theory which concerns our report in these fields will be examined.

2.1 Radar Theory

In this section, we give a brief introduction to how a pulse-Doppler radar works and examine its benefits and limitations. In the last part of the this section, we also investigate the main natural sources of interference which this type of radar system encounters.

2.1.1 Introduction to Pulse-Doppler Radar

More information on this subject can be found in Stimson's *Introduction to Airborne Radar* [3] from where much of the information below is found.

A pulse-Doppler radar works by emitting a high intensity radio signal in a burst with a specific carrier wave frequency. This burst is emitted during a short time, and during the release of the burst the receiver must be turned off since otherwise it might be burned out due to the high intensity of the emitted signal. When the signal has been emitted, the receiver is turned on and starts detecting incoming signals within a narrow bandwidth around the carrier wave frequency of the emitted signal. If an incoming signal is detected within this bandwidth, it could be an echo from a target and the range to the objects which reflected the signal can be calculated by applying equation (2.1), where t is the time between the emitted- and received signal, c is the speed of light and the division with two is included since the signal

has to travel the distance both to the reflecting object and back to the radar.

$$R = \frac{c \cdot t}{2} \tag{2.1}$$

To update the radar image, a new pulse burst is emitted. The time between the pulse bursts is called the pulse repetition interval (PRI) and its inverse is named the pulse repetition frequency (PRF). In the type of pulse-Doppler radar that has been examined in this report the PRF is in the range between 8 to 16 kHz which is a Medium PRF radar [3], and due to this high repetition frequency the change in range between two following pulses is very small and the range can be assumed to be static.

A schematic sketch of a pulse-Doppler radar is given in Figure 2.1. The parts that are included in this picture are a transmitter, duplexer, antenna, receiver, synchroniser and computer. The transmitter modulates the radio wave that is going to be sent with a specific carrier wave and amplifies the outgoing signal which will increase the range to echos of target that can be detected. The duplexer is a switch which either connects the transmitter or the receiver to the antenna. If the duplexer does not turn off the incoming signal to the receiver when the antenna transmits a signal, the receiver might be burned out and damaged. The antenna is either used to transmit the received signal from the transmitter into a well defined radio beam in the area of interest or to detect incoming signals which are then sent to the receiver. The receiver is sensitive to the signals in and around a narrow bandwidth of the transmitted signal's carrier wave and these incoming signals that are within the bandwidth are amplified. The signals are also discretised into different range bins, where the range can be calculated from equation (2.1). The signals are then transferred from the receiver to a computer where signal processing operations are done as well as detection before the operator receives an image of possible targets on a display. The synchroniser is the internal clock of the system which decides when a pulse should be created and sent and when the duplexer should switch so the antenna is used to receive signals instead. The synchroniser is also responsible of informing the receiver when the range bins should be reset which is at the same time as when a new burst is transmitted by the antenna.

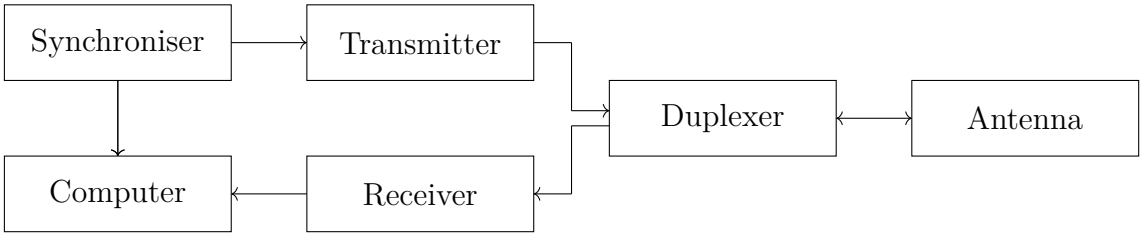

Figure 2.1: A schematic sketch over the different parts in a pulse-Doppler radar.

When more than one pulse burst has been emitted it is hard to know from which emitted pulse the incoming signal is reflected from. One might think that the easiest way is to mark each pulse by changing some parameter in the burst such as the

amplitude, width or frequency in a cyclic way. However changing some of these parameters will lead to new emerging problems which are described on page 156 in Stimson [3].

Instead the PRF is changed after a pre-decided number of bursts has been emitted and received at a specific PRF. By changing the PRF also the maximal unambiguous detection range will be changed as in equation (2.2), which can be derived from equation (2.1).

$$R_{\max} = \frac{c}{2 \cdot PRF} \tag{2.2}$$

By using a new PRF the detected range to a target that lies outside of the maximal unambiguous detection range will change and the true range can be calculated by equation (2.3) where R_1 and $R_{\max_1}$ are the range to an incoming echo from an outgoing pulse and the maximal unambiguous detection range for a specific PRF and then R_2 and $R_{\max_2}$ are detected for a new PRF which is lower than the previous PRF. An illustration of the change is seen in Figure 2.2.

$$n = \frac{R_1 - R_2}{R_{\max_1} - R_{\max_2}} \tag{2.3}$$

$$R_{\text{true}} = n \cdot (R_{\max_1}) + R_1$$

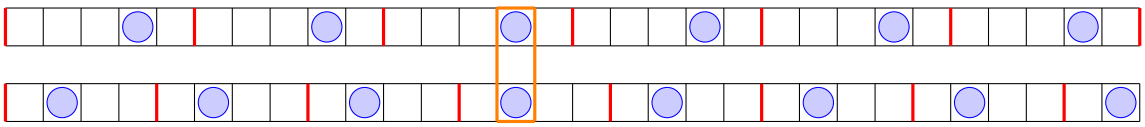

Figure 2.2: An illustration over how the true range to a target range can be detected by changing the PRF. The blue circles represent an echo from a target in a range bin. The changing of the PRF is illustrated by the shift of the red line. By then comparing the signal with the different PRF can the true range be found, which is encircled by the orange square.

If there is more than one target in the radiated area of interest more PRF's will be needed to detect the true range to the targets.

The main advantage of using a pulse-Doppler radar is that by sending out many pulses a shift in frequency can be detected. This shift is induced by the Doppler shift and is thereby related to the velocity of the object which reflected the echo in regard to the radar, and the relation is given in equation 2.4

$$v = -\frac{f_{\text{D}} \cdot c}{2 \cdot f_0} \implies v = -\frac{f_{\text{D}} \cdot \lambda}{2}, \tag{2.4}$$

where f_D is the Doppler shift, f_0 is the carrier wave's frequency and λ is the carrier's wavelength.

By implementing the Nyquist-Shannon theorem to equation (2.4), the largest relative velocity in regard to the radar which can be detected can be calculated as in equation (2.5). Due to this, the real velocity of a target will be ambiguous if a greater resolution than the v_{max} for the velocity is desired.

$$v_{max} = \pm PRF \cdot \lambda/4 \tag{2.5}$$

However the effect of the aliasing of the velocity can be eliminated by changing the PRF which will change the period over which the aliasing occurs and the true velocity can be detected as in equation (2.6) in a similar way as the true range in equation (2.3).

$$n = \frac{f_{D_1} - f_{D_2}}{PRF_1 - PRF_2}, \tag{2.6}$$

$$f_D = f_{D_1} + PRF_1 \cdot n$$

Equations (2.2) and (2.5) can be combined to gain equation (2.7).

$$v_{max} \cdot R_{max} = \pm c \cdot \lambda/8. \tag{2.7}$$

It is seen that the choice of PRF will affect both the maximum velocity and the maximum range which can be detected without aliasing. To gain a good resolution in the range, a low PRF is needed while a good resolution in the velocity needs a high PRF. This relation is called the Doppler dilemma and the choice of the PRF will be a trade-off between the maximum non-ambiguous range and velocity. This relation can be seen in Figure 2.3.

Due to the design of the pulse-Doppler, where the radar both works as a transmitter and receiver there will be some blind spots in the detection. These blind spots arise due to the fact that that the receiver is turned off when a signal is being transmitted. The ranges which are blind are given by equation (2.8).

$$R_{blind} = \frac{c \cdot \Delta t}{2} + n/PRF, \tag{2.8}$$

where Δt is the time it takes to emit a pulse burst and n is an integer going from $0, 1, 2, ..., N_{pulse} - 1$, where N_{pulse} is the number of pulses which are emitted with the same PRF. So the change of the PRF in a pulse-Doppler radar will not only resolve

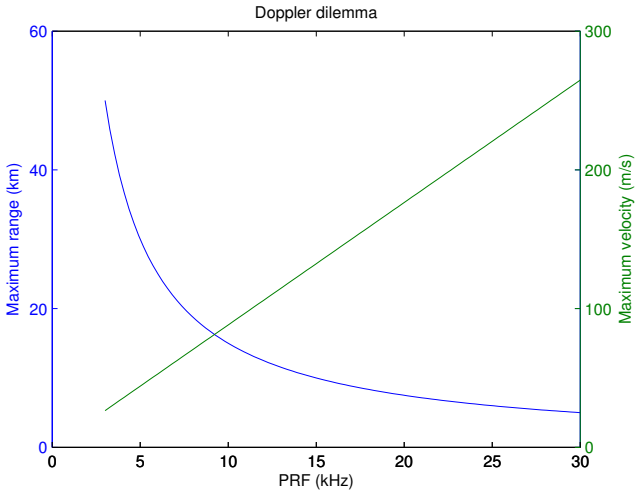

Figure 2.3: In this figure, it is illustrated how the maximum unambiguous range and velocity depends on the PRF. Equation (2.2) and (2.5) have been used with a carrier wave with a frequency of 8.5 GHz.

the ambiguity in velocity and range but also help to change the blind spots which is a very attractive attribute for a radar. However, since more than one PRF is needed the time needed to radiate each area of interest will be increased.

2.1.2 Noise & Disturbances

One of the most important parameters of a radar is at which maximum range a target can be detected. In this thesis only the X-band in the radar is studied (7-11.2 GHz). The carrier waves, in the X-band, are electromagnetic radiation and thus can not penetrate liquid and solids very far, however they have the main advantage that they are good at propagating in air and penetrating through clouds [3]. Due to this, the maximum range is intrinsically limited to the line of sight without any interfering objects.

But even if the target is within the line of sight it might not be detectable since other signals can be interfering such as ground clutter, interference (as other radars operating in the same bandwidth), low radar cross-section (RCS) and background noise.

The main sources of the background noise are the electrical noise from the receiver and the thermal noise from the ground, atmosphere and sun which are within the receiver's bandwidth [3].

From these noises a mean noise energy can be estimated which is given by equation (2.9).

$$N_{\text{mean}} = k \cdot T_{\text{s}}, \tag{2.9}$$

where k is the Boltzmann constant and T_{s} is the noise temperature which includes all of the different types of noise seen in the system. The received signal energy from an echo of one pulse can be calculated as in equation (2.10) [3].

$$E_{\text{signal}} = \frac{P_{\text{avg}} G \sigma A_{\text{e}} \tau}{(4\pi)^2 R^4}, \tag{2.10}$$

where P_{avg} is the average transmitted power, G is the antenna gain, σ is the radar cross section of the target, A_e is the effective area of the antenna which is used to receive signals, τ is the pulse width of the transmitted pulse and R is the range to the target.

If we assume that there is no other interference than the background noise, the maximal range of detection can be calculated by combining equation (2.9) and (2.10) to equation (2.11), found as

$$R_{\text{max}} = \sqrt[4]{\frac{P_{\text{avg}} G \sigma A_{\text{e}} \tau}{(4\pi)^2 S_{\text{min}}}} \propto \sqrt[4]{\frac{P_{\text{avg}} G \sigma A_{\text{e}} \tau}{k \cdot T_{\text{s}}}}, \tag{2.11}$$

where S_{min} is the smallest strength of a signal that can be detected and is related to noise level.

This equation is a form of the famous Radar range equation (at least in radar circles) included to highlight that the return of the received signal is very small in comparison with the outgoing signal and scales with R^{-4}. This received signal also has to compete with the noise which emerges due to the environment in which the radar operates as well as with the intrinsic noise from components in the radar system.

In real world problems one also encounters a type of natural disturbance which is the received reflection from the ground.

In the focusing process of the outgoing radar beam, most of the outgoing energy is focused in the main lobe but a small portion of the energy will also be sent out as side lobes, the cross-section of the outgoing radar signal is shown in Figure 2.4. [3]

When the main beam interferes with the ground, a return which is called the main beam clutter (MBC) will emerge. Since the main lobe is the strongest outgoing lobe from the radar, this return will generally be very high, much higher than the returning signal from a target and this is even true for a radar at a high altitude which directs the main lobe straight forward into the air [3]. The Doppler frequency of any echo can be calculated from equation (2.12).

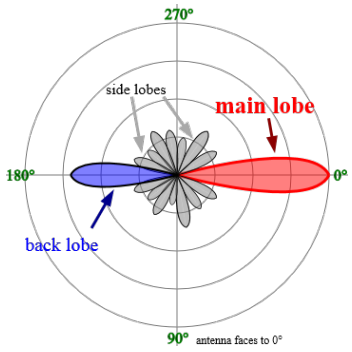

Figure 2.4: A cross-section of the outgoing radar wave from the antenna. The main lobe is the desired beam but due to diffraction one also gets side lobes and a back lobe as seen in this figure. (Source: Wikipedia, `https://en.wikipedia.org/wiki/Main_lobe`)

$$f_{\mathrm{D}} = \frac{2v_{\mathrm{R}}\cos(L)}{\lambda}, \tag{2.12}$$

where v_{R} is the velocity of the radar in regard to the object producing the echo, L is the angle between the velocity direction of the radar and the point of the echo, while λ is the wavelength of the carrier wave.

The side lobes will be directed all around and return an echo from the ground to the radar. This clutter is known as the side lobe clutter (SLC). The Doppler frequencies of this return can also be calculated from equation (2.12), and since they are spread around in all directions their Doppler frequency will be in the whole interval between $-2v_{\mathrm{R}}$ to $2v_{\mathrm{R}}$ but mostly concentrated around 0 f_{D}.

A scenario of how the ground clutter from the main beam and side lobes interfere with the receiving signals from targets is in Figure 2.5. Depending on the velocity of the targets they might be easier or harder to detect. Target A has a velocity relative to the radar of $-2v$ and will not be affected by the ground clutter from the main lobe or side lobe. Target B is flying perpendicular to the radar and the relative velocity between the radar and target B will be v. Target B will then have the same Doppler frequency as the main beam clutter and the target will be hard to detect due this. Target C is moving in the same direction and with the same speed as the radar, due to this will the relative velocity between the radar and target C be the same as the relative velocity between the radar and ground signal attained from the side lobe clutter. Also in this case it will be hard to detect the target due to the side lobe clutter.

It is seen that a pulse-Doppler radar will be able to detect very small returning echos from targets which do not lie close to the clutter frequencies since the ground clutter will not interfere with these signals while some small Doppler frequency intervals will be almost blind since all the ground clutter is shifted into these regions.

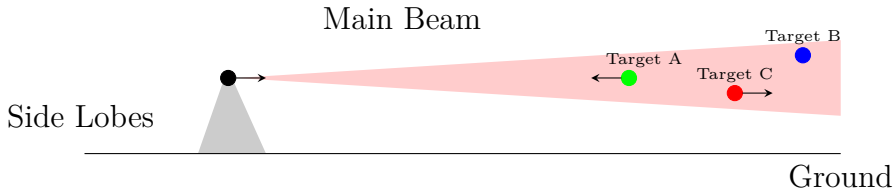

Figure 2.5: In this figure we see a radar (black circle) moving forward with the speed of v and sending out a radar signal in the main lobe and side lobe. Three targets are illuminated by the main lobe. Target A moving towards the radar with the speed of v, target B is flying in a perpendicular direction to the radar and target C is flying in the same direction as the radar and with the same velocity.

2.1.3 Interference

The radar pulse sent from the aircraft to identify targets first scales with R^{-2}, where R is the range the pulse has travelled, due to expanding as part of a spherical area. When this signal is then reflected on the surrounding area these points of reflection will become new point sources emitting echoes in a similar spherical area thus once again scaling with R^{-2} and therefore the target return power will scale with the resulting R^{-4}. Jamming of the radar from another aircraft is only scaling with R^{-2} and will, after a certain range, be much stronger than the target signal as can be seen in Figure 2.6. The range where the target return is distinguishable from the jamming noise is called the burn-through and is also illustrated in the figure.

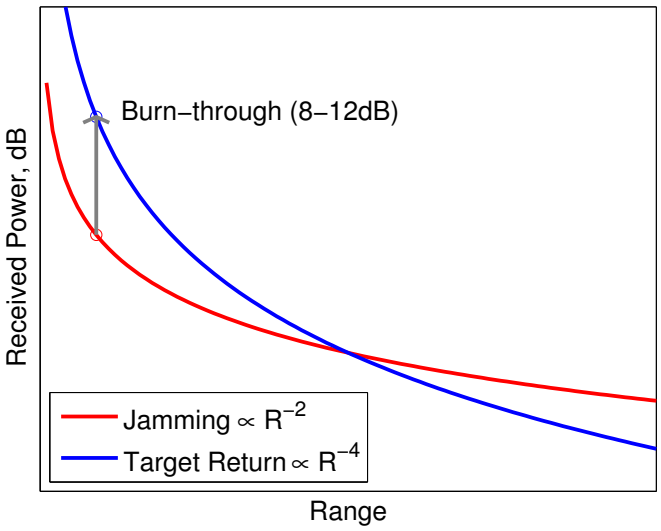

Figure 2.6: The burn-through, represented by the gray arrow, can be seen in this figure. This is where the target will be identifiable through the jamming noise.

Sometimes, also other nearby radars' carrier waves will be in the bandwidth of our radar. This will lead to that very strong signals will be received and hamper the Doppler spectrum.

2.2 Signal Processing

Because one can not change the physics of the world it is hard to improve the physical radar. Thus to improve the quality of the radar data one has to turn to signal processing and use methods such as detection, suppressing noise and filtering. Here, the focus is to describe simple methods of filtering and detection. This is however not used before our algorithms and thus not studied in depth.

2.2.1 Windowing & Zero-Padding

Before performing a Fast Fourier Transform (FFT), zeros can be added to the vector of the signal. This is called zero-padding. These added zeros will not contribute with any new information but they will contribute in the way that the FFT result has more closely spaced frequency bins and produce a smoother looking spectrum[4]. For a pulse-Doppler radar the spacing between the frequencies is given by $\Delta f = F_S/N$, where F_S is the sampling frequency which is the same as the PRF and N is the number of data points which is increased by the added zeros[4]. Zero-padding can also be used to show how the spectral leakage looks which is illustrated in Figure 2.7.

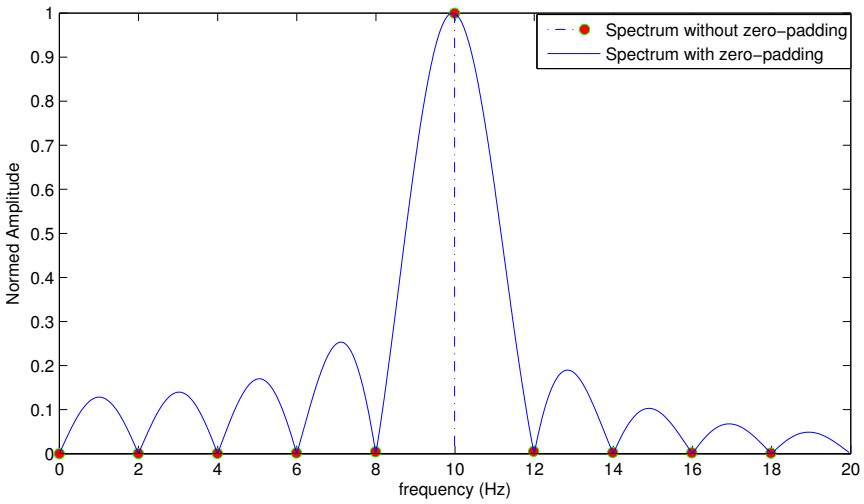

Figure 2.7: The red circles are obtained from a sine function with the frequency of 10 Hz for the time between $[0, 0.5]$ and a sampling frequency of 2048 Hz. The blue signals are obtained by doing a FFT to the same signal which has been zero-padded by adding $1024 \cdot 10^2$ additional zeros before the FFT. In the zero-padded spectrum the leakage from the 10 Hz is clearly seen and the zero-padded spectrum is smoother than the spectrum which is not zero-padded.

The leakage emerges since when performing a FFT over a closed interval the incoming signal can be seen as the multiplication of two signals, namely the continuous

and infinite representation of the original input sinus signal and a rectangular window. The Fourier transform of this resulting function can then be described by the convolution of the two functions. Thus the ringing emerges from the Fourier transform of the rectangular window. This is illustrated in Figure 2.8. If we assume that the original signal is an ordinary sine wave (as in the figure above), then its FFT results in a single value at the sine wave's frequency as the red circles in Figure 2.7 since 10 Hz is periodic in the interval from [0,0.5], while the FFT of the rectangular window will give rise to the $\sin(\pi x)/\pi x$ and their convolution is the blue spectrum seen in Figure 2.7.

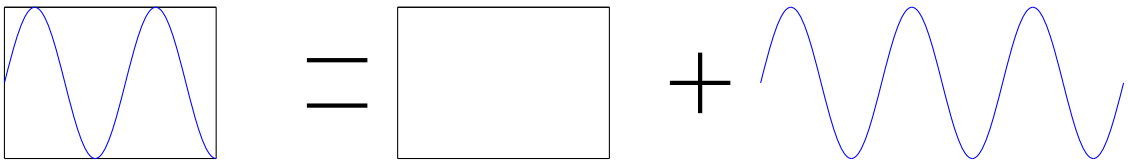

Figure 2.8: A FFT is a convolution of a rectangular window and an infinite signal in the time domain.

If we instead use a non periodic signal over the interval as a sine function with the frequency of 9.5 Hz, it is seen that we do not retrieve a delta function for the spectrum which is not zero-padded since the signal is not periodic over the interval and will be smeared out as in Figure 2.9.

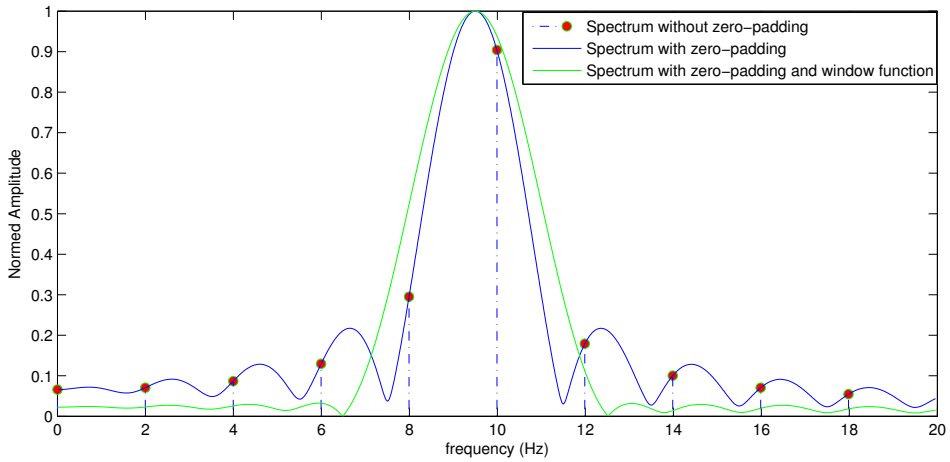

Figure 2.9: The red circles are obtained from a sine function with the frequency of 9.5 Hz for the time between $[0, 1]$ and a sampling frequency of 2048 Hz. The blue signals are obtained by doing a FFT to the same signal which has been zero-padded by adding $1024 \cdot 10^2$ additional zeros before the FFT. The green spectrum is obtained by adding a Taylor window to the to the original signal and then zero-padding the signal as previously. It is seen that the Taylor window will suppress the side lobes while broadening the main lobe.

To minimise the leakage effect, we use a window function. The task of the window is to form a finite length sequence of an infinite length sequence by multiplying

the signal with the window. The window function of the discrete FFT on a closed interval, from where the ringing emerges, can be described as

$$w(n) = \begin{cases} 1 & \text{if} \quad 0 < n < M - 1 \\ 0 & \text{otherwise,} \end{cases}$$

where M is the length of the signal. There is a big variety of different windowing functions and the reason to use them is to change the characteristics of the leakage which is a trade off between broadening the main lobe and suppressing side lobes. In chapters 3 and 4 we used a Taylor window which is a window function which produces the narrowest main lobe for a specified maximum side lobe level when the number of samples in the vector is known [5].

The effect of a Taylor window compared with a rectangular window is seen in Figure 2.9 where it is clearly seen that the main lobe is broader for the Taylor window while the side lobes are lowered compared with rectangular window which is imposed since we do not have an infinite sample in the time domain.

2.2.2 Moving Target Identification

The purpose of a moving target identification filter (MTI) is to remove the low frequencies in the spectrum in part because they are generally not targets of interest but more importantly, to reduce the main beam clutter which is generally in the low frequencies and will greatly affect the frequency spectrum. One of the simpler MTI filters is the binomial MTI filter. A 2-pulse MTI filter is applied by taking the signal value at the discrete time t and removing the signal value at $t - 1$ so that $y_t = x_t - x_{t-1}$. Since the impulse response from this filter is $h_t = \delta_t - \delta_{t-1}$ the Fourier transform of this is $H(\omega) = 1 - e^{-i\omega}$ where $\omega = 2\pi f$. From this function it is seen that the filter suppresses the most at frequencies $2\pi n$ periodically for $n = 0, 1, ...,$ and so on. The frequency response $H(\omega)$ can be seen in Figure 2.10. However it will also increase the magnitude of the frequencies in the centre of the frequency spectrum compared to those closer to the edges.

2.2.3 Constant False Alarm Rate (CFAR)

CFAR is a detection method suitable for detecting targets in a pulse-Doppler radar. This detection method studies the Doppler frequency spectrum and compares each data sample to the area around it and determines if it is a target or not depending on a threshold value.

There are many different types of CFAR. However a simple and common algorithm works by evaluating a cell (a data saple) in the frequency domain and the first few

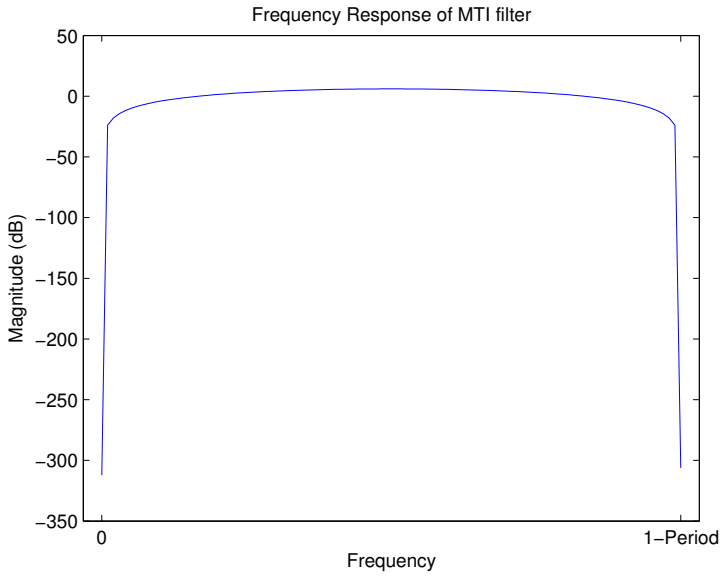

Figure 2.10: The frequency response of the MTI filter in dB over one period. Here the MTI filter reduces the effect of the frequencies in the beginning and the end of the period (the low frequencies).

samples around this cell are guard cells. These cells will be ignored and the number of guard cells are set with a parameter value. The next parameter value are the training cells which will be evaluated and compared to the cell under test. The average value over the training data cells are calculated as,

$$P_n = \frac{1}{N} \sum_{m=1}^{N} x_m,$$

where x_m is the training cell m, and N is the number of training cells. From this the threshold is calculated as $\alpha = N(P_{fa}^{-1/N} - 1)$, where P_{fa} is a chosen parameter of the desired probability of false alarm.

If the energy of the evaluated cell (P_n) is stronger than the calculated threshold from the training set this algorithm will indicate that there is a target in the cell.

A one dimensional example of how the CFAR works is seen in Figure 2.11, it is required that the noise is kept at a low level compared with the target for the CFAR algorithm to work in a satisfying way.

2.2.4 Example Scenario

For demonstrative purposes, an example scenario of simulated radar data can be seen in Figure 2.12. Without any disturbances other than MBC and side lobe clutter (SLC) a simple method to reduce the effect of the MBC and make it easier for the

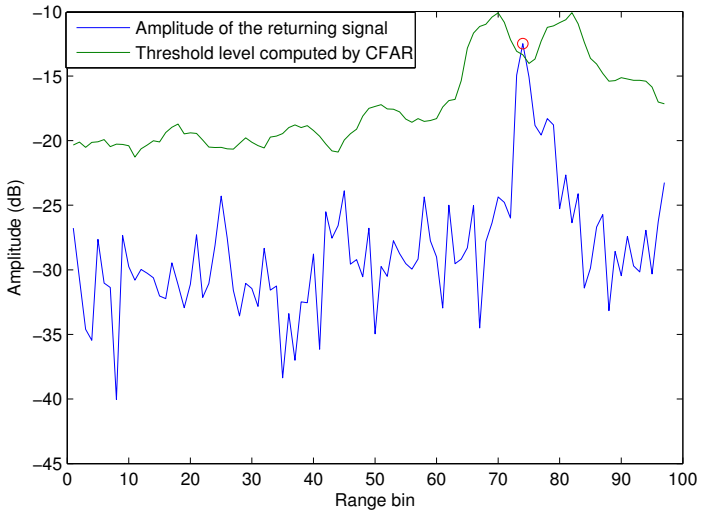

Figure 2.11: In this figure the amplitude of the returning signal is seen at a certain range. From the incoming signal a threshold level is computed with four guard cells (two at each side), fourteen training cells and a false alarm probability of 5 %. It is seen that the CFAR detection method, used here, indicates one possible target which is marked with a red ring.

target to be detected using CFAR detection is shown. First since the direction of the main lobe is known as well as the velocity, it is also known where the MBC should be and can thus be shifted to zero frequency. The shift is done by multiplying the signal in the time domain with $e^{i \cdot \omega_{shift} \cdot t}$, were ω_{shift} how much to shift. This originates from the Fourier transform as $\mathscr{F}[f(t) \cdot e^{i\omega_0 t}] = F(\omega - \omega_0)$ [6]. Also notice in this example that central frequencies are slightly enhanced from the MTI filter. This thesis does not study better methods to take care of MBC or SLC, our purpose will be to reconstruct data before this processing. However the focus is mainly on data with strong MBC and without SLC.

2.3 Missing Data Algorithms

The main concern of this thesis is to estimate the frequency spectrum of an incoming complex signal, in the time domain, which for some reasons is missing some of its data points. One of the reasons why the data is missing could be due to that it is corrupted by an interfering signal as by an asynchronous interference from another radar or radar jammer. This interference could create false targets and also real targets could go missing. Since the data is missing there is no possible way of extracting more information than there is in the uncorrupted data samples. Consider an example where there are 50 missing data samples from a total of 100 data samples but the missing ones are the last 50 samples. In this case the best thing to do would be to perform a FFT over the first 50 samples and thus receiving

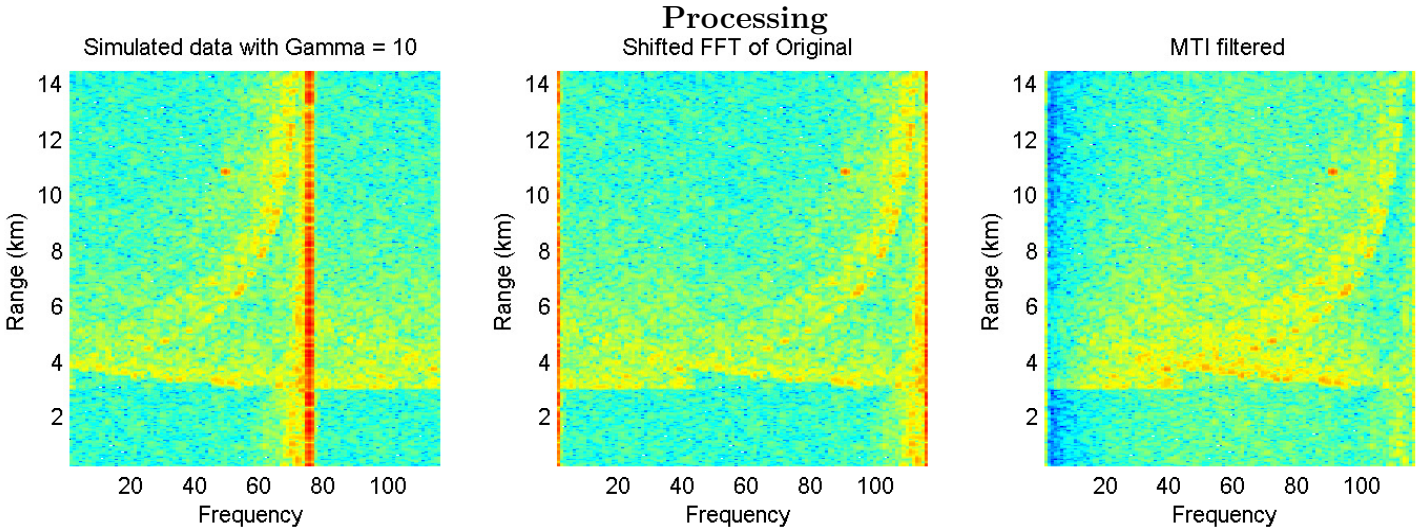

Figure 2.12: An example scenario of a simple method of reducing MBC so that target detection can be made. The left image shows what the simulated data looked like with $\gamma = 10$, which is a parameter determining the magnitude of the ground clutter. In the figure in the middle, the data is shifted in the frequency domain so the MBC will be positioned at zero. This will enable the use of the MTI filter which will filter out low velocity targets relative to the ground, which is seen in the right figure. Most important is to reduce the magnitude of the MBC. Notice that MTI filter enhances the SLC which will have to be dealt with differently

the best estimated spectrum from the data points. But if there are only a few uncorrupted consecutive data points this method is not satisfying since there may be a large frequency correlation between the given data points which are separated by corrupted data samples. This is the problem we have at hand to solve. To solve this missing data algorithms are implemented, which strives to estimate the frequency spectrum from the given data set where some of the data is missing.

The algorithms studied here are of two types: iterative adaptive approach (IAA) and compressive sensing (CS). There are two algorithms studied for CS which are CAMP and a primal-dual algorithm for the L_1 minimisation.

2.3.1 Compressive Sensing

The main principle behind compressive sensing (CS) is that if one rewrites the signal in a suitable basis there are a few dominating bases which can reconstruct the signal. Thus it uses the same principle as is used for compressing data, hence the name. For example a signal can be perfectly reconstructed with a Fourier series, but instead of having infinitely many frequency bases constructing the signal they can usually be heavily reduced down to a few dominant frequency bases which will in a satisfying way reconstruct an approximation of the original signal by using far fewer frequencies[7].

This CS algorithm will only work for signals which are sparse in a domain which is incoherent with the domain the signal is represented in with the missing data. This work was accomplished and proved by Emmanuel Candès, Terence Tao, and David Donoho around 2004 [7].

An equation system is constructed as in equation (2.13), where $\widetilde{A}$ is a $N \times N$ matrix which contain a Fourier basis in each column with length N and can be constructed from the Inverse Fast Fourier transform. $\mathbf{x}$ can be represented by $x_k = \frac{2 \cdot \pi \cdot k}{N}$, where $k = 0, 1, .., N-1$. $\tilde{\mathbf{y}}$ is the received signal, which for some reason contains M missing data points which individually are represented by $\mathbf{0}$.

$$\tilde{\mathbf{y}} = \widetilde{A}\mathbf{x} \tag{2.13}$$

Due to the missing data points in $\tilde{\mathbf{y}}$, a new vector $\mathbf{y}$ and matrix A are constructed by simply removing the missing data points from $\tilde{\mathbf{y}}$ and the corresponding rows from $\widetilde{A}$. This give the dimensions of A, $\mathbf{x}$ and $\mathbf{y}$ as $(N - M) \times N$, N and $(N - M)$ and the system is an undetermined linear system.

Estimating the frequencies ($\mathbf{x}$) in the underestimated equation system is done by introducing an L_1 minimisation. By using the L_1 minimisation it is assumed that the signal will be sparse in frequency and the problem will be convex instead of having infinitely many solutions which is illustrated in Figure 2.13 together with the L_2 minimisation for a two dimensional problem.

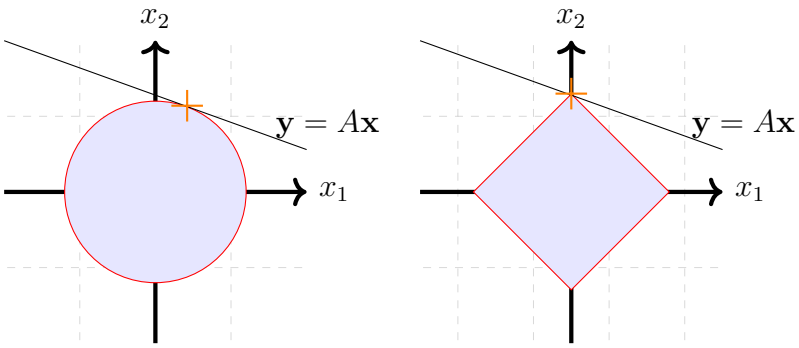

Figure 2.13: These figures are meant to illustrate why an L_1 minimisation will be more sparse than an L_2 minimisation. We have an equation system $\mathbf{y} = A\mathbf{x}$ which is an overestimated system of equations with infinitely many solutions unless another demand is introduced such as an L_1 minimisation (right), or an L_2 minimisation (left). The solution to the systems, with the different demands, is visually presented by the orange cross.

2.3.2 L_1 Minimisation

The L_1 norm minimisation is the problem of,

$$\min ||\mathbf{x}||_1, \quad \text{subject to} \quad A\mathbf{x} = \mathbf{y}. \tag{2.14}$$

In the compressive sensing problem one actually wants to minimise the L_0 norm, which is NP-hard, but because of the property of the sensing matrix it will be equivalent to a L_1 minimisation [8]. To get around this problem there are different algorithms to quickly approximate the best solution to the L_1 minimisation problem. Two CS algorithms, which solve the L_1 minimisation in two different ways, will be presented and an introduction to how the they work will be given.

2.3.3 Primal Dual Compressive Sensing (PD)

One way to perform the L_1 minimisation is by the primal-dual interior-point method. This method is outlined in chapter 11 of Boyd and Vandenberghe's book *Convex Optimisation* and has been followed carefully through this section [9]. However due to limitation in time and space our explanation of the algorithm is not as stringent as in the book.

To start off, equation (2.14) can be rewritten in standard linear form (2.15), by introducing auxiliary variables $\mathbf{u} \in \mathbb{R}^{\mathbf{N}}$ [1] as $\mathbf{z} = [\mathbf{x}, \mathbf{u}]^{\mathbf{T}}$. This is seen in equation (2.16)

$$\min_{\mathbf{u}} \quad \mathbf{c}_0^T \mathbf{z} \quad \text{subject to} \quad A_0 \mathbf{z} = \mathbf{b} \quad \& \quad f_i(\mathbf{z}) \leq 0, \tag{2.15}$$

$$\min_{\mathbf{u}} \quad \mathbf{1}^T \mathbf{u} \quad \text{subject to} \quad A\mathbf{x} = \mathbf{y} \quad \& \quad f_i(\mathbf{x}, \mathbf{u}) \leq 0, \tag{2.16}$$

where $\boldsymbol{x} \in \mathbb{R}^N$ and $\boldsymbol{y} \in \mathbb{R}^M$. f_i are linear functionals of the form given in equation (2.17). [9]

$$f_i(\mathbf{z}) = \langle c_i, \mathbf{z} \rangle + d_i. \tag{2.17}$$

At the optimal solution $\mathbf{z}^*$ there will exist dual vectors $\boldsymbol{\nu}^* \in \mathbb{R}^{\mathbf{M}}$ and $\boldsymbol{\lambda}^* \in \mathbb{R}^{\mathbf{N}}$, given by the duality function to the primal equation (2.15), which fulfils the Karusch-Kuhn-Tucker (KKT) conditions, seen in equation (2.18).[9]

$$\begin{aligned} \mathbf{c_0} + A^T \boldsymbol{\nu}^* + \sum_i \lambda_i^* c_i &= \mathbf{0} \\ \lambda_i^* f_i(\mathbf{z}^*) &= 0 \quad i = 1, 2 \\ A_0 \mathbf{z}^* &= \mathbf{b} \\ f_i(\mathbf{z}^*) &\leq 0, \quad i = 1, 2 \end{aligned} \tag{2.18}$$

[1] This method can also be used for complex data by dividing the problem into two problems, one for the real numbers and one for the imaginary numbers which has been done in the code which is used in the result.

The way to find the optimal solution is by linearising the system at an interior point and then solve the linear equations and find the search directions $\Delta\mathbf{z}$, $\Delta\boldsymbol{\lambda}$ and $\Delta\boldsymbol{\nu}$. But the search directions are not always feasible except in the limit as the algorithm converges. To gain a smooth central path to the optimal solution is a complementary slackness condition introduced to the central path condition as

$$\boldsymbol{\lambda}^*\mathbf{f}(\mathbf{z}) = -1/\tau^k,$$

where τ^k is increased for every new iteration.

The primal, dual and central residuals can be expressed as in equation (2.19) and they give a value of how close the KKT conditions are to being fulfilled,

$$\begin{aligned} \mathbf{r}_{\text{prim}} &= A_0\mathbf{z} - \mathbf{b} \\ \mathbf{r}_{\text{dual}} &= \mathbf{c_0} + A_0^T\boldsymbol{\nu} + \sum_i \lambda_i c_i \\ \mathbf{r}_{\text{cent}} &= -\Lambda\mathbf{f} - (1/\tau)\mathbf{1} \end{aligned} \tag{2.19}$$

where $\Lambda_{ii} = \lambda_i$ and $\mathbf{f} = (f_1(\mathbf{z}), ...f_m(\mathbf{z}))^T$.

The residuals can now be linearised by the Taylor expansion of $\mathbf{r}_\tau = [\mathbf{r}_{prim}, \mathbf{r}_{dual}, \mathbf{r}_{cent}]^T$ which fulfils

$$\mathbf{r}_\tau(\mathbf{z} + \Delta\mathbf{z}, \boldsymbol{\nu} + \Delta\boldsymbol{\nu}, \boldsymbol{\lambda} + \Delta\boldsymbol{\lambda}) = \mathbf{0}, \tag{2.20}$$

and gives

$$\mathbf{r}_\tau(\mathbf{z} + \Delta\mathbf{z}, \boldsymbol{\nu} + \Delta\boldsymbol{\nu}, \boldsymbol{\lambda} + \Delta\boldsymbol{\lambda}) \approx \mathbf{r}_\tau(\mathbf{z}, \boldsymbol{\nu}, \boldsymbol{\lambda}) + J_{\mathbf{r}_\tau}(\mathbf{z}, \boldsymbol{\nu}, \boldsymbol{\lambda}) \begin{pmatrix} \Delta\mathbf{z} \\ \Delta\boldsymbol{\nu} \\ \Delta\boldsymbol{\lambda} \end{pmatrix} \tag{2.21}$$

where $J_{\mathbf{r}_\tau}(\mathbf{z}, \boldsymbol{\nu}, \boldsymbol{\lambda})$ is the Jacobian matrix of $\mathbf{r}_\tau$. We find the linear system in equation (2.22) by combining equation (2.20) and equation (2.21)

$$\begin{pmatrix} A_0 & 0 & 0 \\ -\Lambda C & 0 & -F \\ 0 & A^T & C^T \end{pmatrix} \begin{pmatrix} \Delta\mathbf{z} \\ \Delta\boldsymbol{\nu} \\ \Delta\boldsymbol{\lambda} \end{pmatrix} = - \begin{pmatrix} A_0\mathbf{z} - \mathbf{b} \\ -\Lambda\mathbf{f} - (1/\tau)\mathbf{1} \\ \mathbf{c_0} + A_0^T\boldsymbol{\nu} + \sum_i \lambda_i c_i \end{pmatrix}, \tag{2.22}$$

where C is a $n \times M$ matrix with c_i^T as rows and $F_i = f_i(\mathbf{z})$. This can be simplified by extracting $\Delta\boldsymbol{\lambda}$ as in equation (2.23)

$$\Delta\boldsymbol{\lambda} = -\Lambda F^{-1} C\Delta\mathbf{z} - \boldsymbol{\lambda} - (1/\tau)\mathbf{f}^{-1}, \tag{2.23}$$

which reduce the linear system to

$$\begin{pmatrix} -C^T F^{-1} \Lambda C & A_0^T \\ A_0 & 0 \end{pmatrix} \begin{pmatrix} \Delta \mathbf{z} \\ \Delta \boldsymbol{\nu} \end{pmatrix} = \begin{pmatrix} \mathbf{b} - A_0 \mathbf{z} \\ -\mathbf{c_0} - A_0^T \boldsymbol{\nu} + (1/\tau) C^T \mathbf{f}^{-1} \end{pmatrix}. \tag{2.24}$$

Now the step directions $\Delta \mathbf{z}$, $\Delta \boldsymbol{\nu}$ and $\Delta \boldsymbol{\lambda}$ can be deduced, but we will still need to decide a step length s in the interval $0 < s < 1$, which fulfils the following demands:

1. $\mathbf{z} + s\Delta \mathbf{z}$ and $\boldsymbol{\lambda} + s\Delta \boldsymbol{\lambda}$ are still in the interior of $f_i(\mathbf{z} + \Delta \mathbf{z}) < 0$ and $\lambda_i > 0$ for all i.

2. The norm of the residual has decreased sufficiently:

$$||\mathbf{r}_\tau(\mathbf{z} + s\Delta \mathbf{z}, \boldsymbol{\nu} + \Delta \boldsymbol{\nu}, \boldsymbol{\lambda} + \Delta \boldsymbol{\lambda})||_2 \leq (1 - \alpha s) \cdot ||\mathbf{r}_\tau(\mathbf{z}, \boldsymbol{\nu}, \boldsymbol{\lambda})||_2$$

   where α is a choosable parameter.

$s_{\max}$ is decided as

$$\begin{aligned} s_{\max} &= \sup\{s \in [0,1] \quad | \quad \boldsymbol{\lambda} + s\Delta \boldsymbol{\lambda} \succeq 0 \quad | \quad \mathbf{f}(\mathbf{z} + \Delta \mathbf{z}) \preceq 0\} \\ &= \min\{1, \min\{-f_i(\mathbf{z})/\Delta \mathbf{z} | f_i(\Delta \mathbf{z}) > 0\}, \min\{-\lambda_i/\Delta \lambda_i | \Delta \lambda_i < 0\}\}, \end{aligned}$$

where $\min\{-f_i(\mathbf{z})/\Delta \mathbf{z} | f_i(\Delta \mathbf{z}) > 0\}, \min\{-\lambda_i/\Delta \lambda_i | \Delta \lambda_i < 0\}$ is given by the infeasible Newton method. [9]

s is initiated to $0.99 s_{\max}$ and if it fulfils the two demands seen above, we update $\mathbf{z}$, $\boldsymbol{\nu}$ and λ, else we multiply s with β which usually is in the range $[0.3, 0.8]$ and we have used 0.5 in our algorithm.

The convergence is decided by the surrogate duality gap which is given in equation (2.25), and when this is below a given threshold the algorithm is done.

$$\eta = -\mathbf{f^T} \boldsymbol{\lambda} \tag{2.25}$$

For a L_1 minimisation are the functionals are given as in equation (2.26)

$$\begin{aligned} \mathbf{f}_1(\mathbf{u}, \mathbf{x}) &\equiv x_i - u_i, \\ f_2(\mathbf{u}, \mathbf{x}) &\equiv -x_i - u_i, \end{aligned} \tag{2.26}$$

where $\mathbf{u}$ [2] is initiated to a value which fulfils $f_i(\mathbf{x}) \leq \mathbf{0}$ for $i = \{1, 2\}$. [10]

[2] In our algorithm is $\mathbf{u}$ initiated to $(0.95) \cdot |\mathbf{x}_0| + 0.1 \cdot max(abs(\mathbf{x_0}))$, where $\mathbf{x_0}$ is an initial guess of the signal in the sparse basis. If the initial guess is not within the interior it is initialised to $A^T(A^2)^{-1} \cdot \mathbf{y}^T$. This is in accordance with [10] and equation (2.26).

Since f_i is given for our problem the two first KKT conditions in equation (2.18) can be written as,

$$\begin{aligned} \begin{pmatrix} \lambda_1 - \lambda_2 + A^T\nu \\ \mathbf{1} - \lambda_1 - \lambda_2 \end{pmatrix} &= \mathbf{0}, \\ \begin{pmatrix} \lambda_1(\mathbf{x} - \mathbf{u}) \\ \lambda_2(-\mathbf{x} - \mathbf{u}) \end{pmatrix} &= \mathbf{0}, \end{aligned} \tag{2.27}$$

where λ_1 is the duality vector corresponding to $\mathbf{f}_1$ and λ_2 is the duality vector corresponding to $\mathbf{f}_2$. We can also rewrite the residuals from equation (2.19) as in equation (2.28)

$$\mathbf{r}_{\text{prim}} = A\mathbf{x} - \mathbf{y} \tag{2.28}$$

$$\mathbf{r}_{\text{dual}} = \begin{pmatrix} \boldsymbol{\lambda_1} - \lambda_2 + \mathbf{A^T}\nu \\ \mathbf{1} - \boldsymbol{\lambda_1} - \boldsymbol{\lambda_2} \end{pmatrix} \tag{2.29}$$

$$\mathbf{r}_{\text{cent}} = -\begin{pmatrix} \boldsymbol{\lambda_1}(\mathbf{x} - \mathbf{u}) \\ \boldsymbol{\lambda_2}(-\mathbf{x} - \mathbf{u}) \end{pmatrix} - \mathbf{1}/\tau^{\mathbf{k}}, \tag{2.30}$$

With the given functionals in (2.26) equation (2.24) can be written as in (2.31)

$$\begin{pmatrix} A & 0 & 0 \\ \Sigma_1 & \Sigma_2 & A^T \\ \Sigma_2 & \Sigma_1 & 0 \end{pmatrix} \begin{pmatrix} \Delta\mathbf{x} \\ \Delta\mathbf{u} \\ \Delta\nu \end{pmatrix} = \begin{pmatrix} \mathbf{y} - A\mathbf{x} \\ (-1/\tau) \cdot (-\mathbf{f}_1^{-1} + \mathbf{f}_2^{-1}) - A^T\nu \\ -\mathbf{1} - (1/\tau) \cdot (\mathbf{f}_1^{-1} + \mathbf{f}_2^{-1}) \end{pmatrix}, \tag{2.31}$$

and from equation (2.23) can $\Delta\lambda$ be deduced. The search directions are now found and the line search that was mentioned earlier can begin.

The pseudo code for this algorithm is given in algorithm (1) and as output is a estimation of the frequency spectrum ($\boldsymbol{x}$) received.

2.3.4 Complex Approximate Message Passing (CAMP)

Another way to solve the L_1 minimisation, and at the same time reduce the effect from inherent noise in the signal, is by using the Complex Approximate Message Passing algorithm (CAMP). In this introductory section to CAMP we have followed chapter 9 in Cheng's book and chapter 9 in Eldar and Kutyniok's book [11] [12]. This algorithm assumes that the signal can be described by (2.32).

Algorithm 1 Primal-Dual Interior Point Method

1: **Input**: $\boldsymbol{y}$, A, f, τ, α & β
2: **Initiation**: $\boldsymbol{x} = A^T \cdot \boldsymbol{y}$, $\eta = \infty$. $\boldsymbol{u} = (0.95) \cdot |\mathbf{x}| + 0.1 \cdot max(abs(\mathbf{x}))$, $\lambda_i = -1/f_i$
3: & $\nu = -A(\lambda_1 - \lambda_2)$
4: **While**: $\eta > \tau$
5: Use equation (2.31) and (2.23) to calculate the search direction $\Delta\mathbf{x}$, $\Delta\mathbf{u}$, $\Delta\nu$ and $\Delta\lambda$.
6: Calculate the step length s by using equation and .
7: Update the variables as $\mathbf{x} = \mathbf{x} + s\Delta\mathbf{x}$, $\mathbf{u} = \mathbf{u} + s\Delta\mathbf{u}$, $\nu = \nu + s\Delta\nu$ & $\lambda = \lambda + s\Delta\lambda$
8: Calculate $\eta = \mathbf{f^T}\lambda$
9: **Output:** $\boldsymbol{x}$

$$\boldsymbol{y} = A\boldsymbol{x} + \boldsymbol{n} \tag{2.32}$$

where $\boldsymbol{y}$, $\boldsymbol{x}$ and A are the same variables as given and explained in equation (2.14), while $\boldsymbol{n}$ is assumed to be a complex Gaussian noise vector with mean 0 and standard deviation $1/\beta$.

We will henceforth use a notation with $p(dx)$, where p stands for the probability measure while d shows which variable is distributed. When we write $p(dx, y)$ we mean the conditional probability measure of x when y is known. When $d\mathbf{x}$ stands by itself without any p it is used to indicate the Lebesgue measurement as in equation (2.33).

$$p(dx) = \frac{1}{\sqrt{2\pi a}} e^{-x^2/2a} dx, \tag{2.33}$$

where a is a bandwidth parameter.

With this formalism equation (2.32) can be written as in equation (2.34) by formulating the problem as a graphical model problem, where the conditional distribution $p(d\boldsymbol{y}|\boldsymbol{x})$ models the noise, while the prior $p(d\boldsymbol{x})$ contains the measure of the signal we want to find.

$$p(d\boldsymbol{x}, d\boldsymbol{y}) = p(d\boldsymbol{y}|\boldsymbol{x})p(d\boldsymbol{x}) \tag{2.34}$$

If we assume that we already know the signal $\mathbf{x}$, it is possible to construct the conditional measure $p(d\mathbf{y}, \mathbf{x})$ as in equation (2.35) since this will be a model of the noise $\mathbf{n}$.

$$p(d\boldsymbol{y}|\boldsymbol{x}) = \left(\frac{\beta}{2\pi}\right)^{n/2} e^{\frac{-\beta}{2}||\boldsymbol{y}-A\boldsymbol{x}||_2^2} d\boldsymbol{y} \tag{2.35}$$

By combining equation (2.34) and (2.35) the joint distribution can be written as in equation (2.36).

$$p(d\boldsymbol{x}) = \prod_{j=1}^{n} p(dx_i) \tag{2.36}$$

The posterior distribution is given by (2.37),

$$p(d\boldsymbol{x}|\boldsymbol{y}) = \frac{p(d\boldsymbol{y}|\boldsymbol{x})p(d\boldsymbol{x})}{p(\boldsymbol{y})} \tag{2.37}$$

and from this the posterior distribution of $\mathbf{x}$ can be defined as in (2.38).

$$p(d\mathbf{x}|\mathbf{y}) = \frac{1}{Z(\mathbf{y})} \prod_{j=1}^{M} e^{-\frac{\beta}{2}||\mathbf{y}-A\mathbf{x}||_2^2} \prod_{i=1}^{N} p(dx_i), \tag{2.38}$$

where $Z(\mathbf{y}) = (2\pi/\beta)^{n/2} p(\mathbf{y})$ is included as normalisation constant so $\int p(d\mathbf{x}|\mathbf{y}) = 1$ and $||\ \mathbf{y} - A\mathbf{x}||_2^2 = \sum_{j=1}^{M} (y_j - A_j^T \mathbf{x})^2$.

If we in somehow could estimate this measure in equation (2.38), we could extract an estimation value of $\mathbf{x}$ as in equation (2.39)

$$\hat{x}(y) = \int \mathbf{x} \cdot p(d\boldsymbol{x}|\boldsymbol{y}). \tag{2.39}$$

A way to estimate $p(d\mathbf{x}|\mathbf{y})$ is by implementing an approximate message passing algorithm (also called belief propagation algorithm) and how this is done is seen in [11] and [12].

The pseudo code for the algorithm is given in algorithm 2 and as output is an estimation of the frequency spectrum ($\hat{x}$) received.

Algorithm 2 CAMP

1: **Input**: $\boldsymbol{y}$, A, τ, $\boldsymbol{x_0}$ & ϵ
2: **Initiation**: $\hat{\boldsymbol{x}}^0 = 0$, $\boldsymbol{z}^0 = \boldsymbol{y}$ & $t = 0$
3: **While** $\{||\hat{\boldsymbol{x}}^t - \hat{\boldsymbol{x}}^{t-1}||_2 > \epsilon\}$
4: t=t+1
5: $\tilde{\boldsymbol{x}}^t = A^H \boldsymbol{z}^{t-1} + \hat{\boldsymbol{x}}^{t-1}$
6: $\sigma_t = std(\tilde{\boldsymbol{x}}^t - \boldsymbol{x}_0)$
7: $\boldsymbol{z}^t = \boldsymbol{y} - A\hat{\boldsymbol{x}}^{t-1} + \boldsymbol{z}^{t-1}\left(\langle \frac{\partial \eta^H}{\partial x_{\mathrm{Re}}}(\tilde{\boldsymbol{x}}; \tau\sigma_t)\rangle + \langle \frac{\partial \eta^H}{\partial x_{\mathrm{Im}}}(\tilde{\boldsymbol{x}}; \tau\sigma_t)\rangle\right)$
8: $\hat{\boldsymbol{x}}^t = \eta(\tilde{\boldsymbol{x}}; \tau\sigma_t)$
9: **Output:** $\hat{\boldsymbol{x}}$

This algorithm was developed by Arian Maleki and for more information about this algorithm than in this brief introduction is found in [13] and [14].

2.3.5 Iterative Adaptive Algorithm (IAA)

Another missing data algorithm is the iterative adaptive algorithm (IAA) [15]. This algorithm starts out by defining the Fourier vectors by time and frequency as, $\boldsymbol{a}_g(w_k) = e^{jw_k\boldsymbol{t}_n}$ and $\boldsymbol{a}_m(w_k) = e^{jw_k\boldsymbol{t}_m}$. Here let $\boldsymbol{t}_n$ denote the times of the given data samples, and $\boldsymbol{t}_m$ the times of the missing data points. Also $\boldsymbol{a_g(w_k)}$ and $\boldsymbol{a}_m(w_k)$ are the Fourier column-vectors of the given and missing data samples respectively. Let $k = 1, ..., K$ where K denotes our chosen grid points for the frequencies with equal spacing and w_k corresponds to those frequencies.

$$\boldsymbol{a}(w_k) = \begin{bmatrix} \boldsymbol{a}_g(w_k) \\ \boldsymbol{a}_m(w_k) \end{bmatrix}, A = [\boldsymbol{a}(w_1)...\boldsymbol{a}(w_K)]$$

The full data vector $\boldsymbol{y}$ of the missing and given data $\boldsymbol{y}_g$, $\boldsymbol{y}_m$,

$$\boldsymbol{y} = \begin{bmatrix} \boldsymbol{y}_g \\ \boldsymbol{y}_m \end{bmatrix},$$

is then modelled by $\boldsymbol{y} = A\boldsymbol{\alpha}$. Thus $\boldsymbol{\alpha} = [\alpha(w_1)...\alpha(w_K)]^T$ is to be estimated. It is estimated with the help of a covariance matrix of the given data to iterate closer to the real value of $\boldsymbol{\alpha}$. The initial value of the covariance matrix R_g is the identity matrix. Let $(\cdot)^H$ denote the complex conjugate transpose. The estimate is then,

$$\boldsymbol{\alpha}(w_k) = \frac{\boldsymbol{a}_g^H(w_k)R_g^{-1}\boldsymbol{y}_g}{\boldsymbol{a}_g^H R_g^{-1}\boldsymbol{a}_g}. \tag{2.40}$$

Next, let $\boldsymbol{P}_k = |\alpha(w_k)|^2$ and update the covariance matrix as,

$$R_g = \Sigma_{k=1}^K \boldsymbol{P}_k \boldsymbol{a}_g(w_k)\boldsymbol{a}_g^H(w_k).$$

When these updates have been iterated enough, the restoration of the missing data $\hat{\boldsymbol{y}}_m$ is done by,

$$\hat{\boldsymbol{y}}_m = \left(\Sigma_{k=1}^K \boldsymbol{h}_{m_k}\boldsymbol{h}_{m_k}^H\right)^{-1}\Sigma_{k=1}^K \boldsymbol{h}_{m_k}[\alpha(w_k) - \boldsymbol{h}_{g_k}^H\boldsymbol{y}_g].$$

The terms $\boldsymbol{h}_{g_k}$, $\boldsymbol{h}_{m_k}$ are defined as,

$$\frac{\boldsymbol{a}^H(w_k)R^{-1}}{\boldsymbol{a}^H(w_k)R^{-1}\boldsymbol{a}(w_k)} \equiv [\boldsymbol{h}_{g_k}^H \, \boldsymbol{h}_{m_k}^H], \tag{2.41}$$

where this is a row vector and $\boldsymbol{h}_{g_k}$ and $\boldsymbol{h}_{m_k}$ has the same number of samples as $\boldsymbol{y}_g$ and $\boldsymbol{y}_m$ respectively. Also the covariance matrix for all the data is estimated as,

$$R = \Sigma_{k=1}^{K} P_k \boldsymbol{a}(w_k)\boldsymbol{a}^H(w_k).$$

Again, the derivation of these equations can be found in [15]. A simple description can be seen below in algorithm 3 where the output ($\mathbf{y_m}$) is an estimation of the missing data. Here a for-loop was used with the maximum number of iterations before the algorithm with break. However if the difference between $\boldsymbol{P}_k$ from the previous iteration and the latest iteration was below a threshold the algorithm would break and be considered to have converged to an acceptable value. This tolerance was chosen to be: tol $= 10^{-4}$ in our cases.

Algorithm 3 IAA

1: **Input**: $\boldsymbol{y}$, $\boldsymbol{t}_m$, $n_{\text{iterations}}$, tol
2: **Initiation**: $R_g = \mathbb{1}$, $\boldsymbol{P}_k = \mathbf{0}$, $\boldsymbol{P}_k^{\text{old}} = \mathbf{0}$
3: **For** $\{n_{\text{iterations}}\}$
4: $\alpha(w_k) = \frac{\boldsymbol{a}_g^H(w_k)R_g^{-1}\boldsymbol{y}_g}{\boldsymbol{a}_g^H R_g^{-1}\boldsymbol{a}_g}$
5: $\boldsymbol{P}_k = |\alpha(w_k)|^2$
6: **If:** $|P_k - P_k^{\text{old}}| <$ tol $\rightarrow$ break For-loop
7: $\boldsymbol{P}_k^{\text{old}} = \boldsymbol{P}_k$
8: $R_g = \Sigma_{k=1}^{K} \boldsymbol{P}_k \boldsymbol{a}_g(w_k)\boldsymbol{a}_g^H(w_k)$
9: **End For**
10: $\hat{\boldsymbol{y}}_m = \left(\Sigma_{k=1}^{K} \boldsymbol{h}_{m_k}\boldsymbol{h}_{m_k}^H\right)^{-1} \Sigma_{k=1}^{K} \boldsymbol{h}_{m_k}[\alpha(w_k) - \boldsymbol{h}_{g_k}^H \boldsymbol{y}_g]$
11: **Output:** $\hat{\boldsymbol{y_m}}$

2.3.6 Linear Interpolation

As our final missing data algorithm we implement a linear interpolation. The linear interpolation works by estimating the value of the missing data in the incoming signal $\boldsymbol{y}$ by a linear interpolation between the given data. From the coordinates (x_0, y_0) and (x_1, y_1) (where $\boldsymbol{x}$ is the index of $\boldsymbol{y}$) of the closest given neighbouring samples on each side of the missing data sample, an estimation of the missing data sample's value (y_2) can be calculated as in equation (2.42).

$$y_2 = y_0 + (x_2 - x_0)\frac{y_1 - y_0}{x_1 - x_0} = \frac{y_0(x_1 - x_3) + y_1(x_2 - x_0)}{x_1 - x_0}. \tag{2.42}$$

This is be done both for the real and imaginary parts of $\mathbf{y}$.

The reason why we choose to use this algorithm is especially to have a reference algorithm to compare the performance of the other algorithms with in the evaluation.

3

Method

In this section we introduce the model that we use to evaluate the performance of the algorithms. The model consists of a reference signal in which we vary the strength of a target and an estimation of a disturbance in which the ratio between the given and missing data is changed.

3.1 Data Model

The incoming signal to our algorithms is given in range and time from the pulse-burst. Due to some interference some of the data will be corrupt and we will assume these are missing to reduce the effect of the interfering signal. We here assume that there only are a few important frequencies/velocities in each range so the signal is sparse in the frequency domain and we can use the algorithms to aquire the frequency spectrum from the incoming data in each frequency bin.

One of the hardest tasks to solve during this thesis has been to quantify the performance of the algorithms. Many parameters of the incoming data affect the performance of the algorithms such as clutter, noise, interference, weather and angle of the radar's search direction. Since there is such a big variation in the data set, it has been hard to quantify when and why our algorithms work as they should. To get around this problem we decided to make our own data model for the incoming signal and then vary the initialised parameters in this model and examine the change of some key parameters of the returned spectrum.

Our initialisation of the signal in the time domain $S(t)$ is a vector with the length of 256 samples and contains a target signal $S_{\text{target}}(t)$, a strong main beam clutter signal $S_{\text{mbc}}(t)$ and a Gaussian distributed noise signal $N(t)$, as given in (3.1). Since this is a constructed signal without a sampling time the extracted frequency spectrum from the FFT and the missing data algorithms can not be converted into Hz or radians per second but will be in relative frequency which is related to the sampling time and the number of samples (or FFT length if zero-padding is used). Due to this the figures in this chapter and the next will not have a unit for the frequency.

$$
\begin{aligned}
S(t) &= S_{\text{mbc}}(t) + S_{\text{target}}(t) + N(t), \\
S_{\text{mbc}}(t) &= \sum_k A_k \cdot e^{2\pi i f_k t + \theta_{\text{random}}}, \\
S_{\text{target}}(t) &= B \cdot e^{2\pi i f_t t + \theta_{\text{random}}}, \\
N(t) &= \frac{N_0}{\sqrt{2}}[N(\mu, 1) \cdot i + N(\mu, 1)].
\end{aligned} \tag{3.1}
$$

For simplicity the strength of the N_0 was set to 1. These factors are part of the normalisation and will only affect different signals strength over the noise level. There was an idea to make a model to choose A_k and f_k depending on how the main lobe would spread and at what angle it would echo from the ground. But only one $A_0 = 40dB$ was chosen at zero frequency with the value of $40dB$ per pulse, which was chosen to be an arbitrarily strong MBC signal from recommendations. In S_{target} a random phase shift is induced, θ_{random}, which is initiated randomly in the interval $[0, 2\pi]$.

For clarification what is considered to be the noise level is,

$$
\text{Noise level} = \frac{1}{n}\Sigma_k |S_k|, \tag{3.2}
$$

where n is the number of samples in the frequency domain which are considered to be noise frequencies as shown (in red) in Figure 3.2. Here S_k is the complex data samples of the signal where k is the set of samples in the red area of the figure.

The square root of two in $N(t)$ comes from adding two Gaussian distributions, one for the real numbers and one for the complex. We then assume that there is interference in the signal which creates corrupted data samples and that these can be located so we can apply our data-recovery algorithms together with an appropriate window function to find the frequency spectrum. The type of disturbances which have been examined are either random or periodic and the parameter that is examined and varied is the duty factor which is the fraction of the disturbed samples in regard to the whole signal. For the periodic disturbance in our model, we use a band of corrupted data samples with the length of 5 and randomly initiate the start of the disturbance between the length of the band. This type of disturbance resembles an interfering signal from another radar with a lower PRF. The random disturbance is used to simulate the type of disturbance which could be encountered if many radars at the same time are operating within a small area with a similar carrier wave. A visualisation of the simulated disturbances can be seen in Figure 3.1. We have analysed data from other simulated models as well but for evaluating the algorithms the focus was on our own simple model.

Normalising the system is done by taking into account, N_0, the windowing function, and the number of samples N_s. The strength of a signal increases with the amount

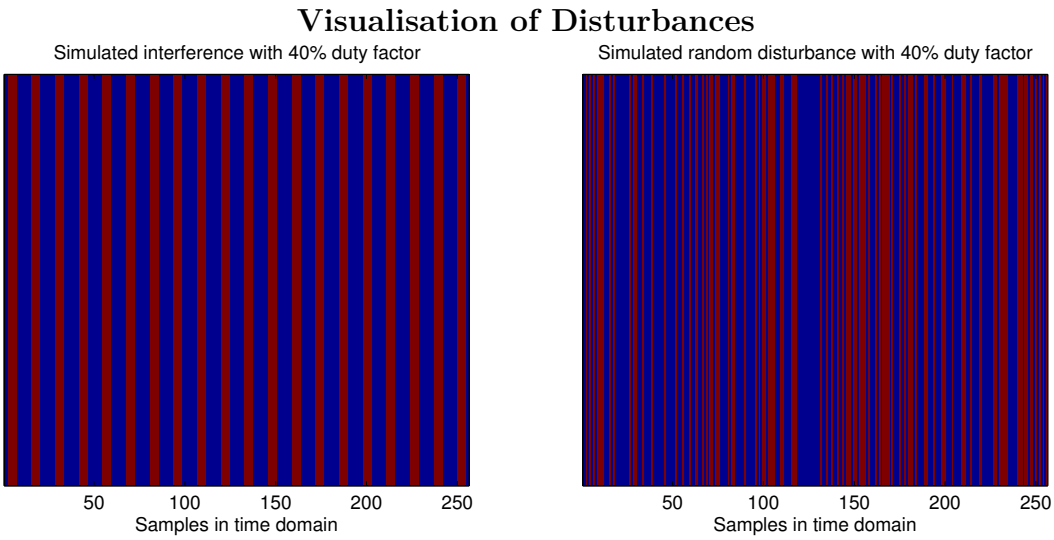

Figure 3.1: Visualising the disturbances for the signals in the time domain. Red are the removed data samples and blue are the data samples from which recovery is made. Note that these disturbances are here shown for one range bin. However recovery for a matrix of range-time data would be done for each range-bin. The interference to the left is periodic with each corrupted band covering 5 data points. This represents a disturbance at one range bin so the images are just a representation of a row vector.

of data-samples where the signal is returned. For a sinus-signal the strength scales with N_s. So if, for example, the target strength is chosen to B per pulse as in equation 3.1, then the expected amplitude in the frequency spectrum is expected to be $B \cdot N_s$. However, Gaussian noise only scales with $\sqrt{N_s}$. So if we want to normalise the system to keep the noise level at 0 dB we divide by $\sqrt{N_s}$. When also taking the noise level N_0 into account, the normalising coefficient becomes $C_{\text{norm}} = N_0\sqrt{N}$ and can be calculated from the scaling of Gaussian noise [6]. Thus the strength of the signal is $\mathscr{F}[\frac{S_{\text{mbc}}(t)}{C_{\text{norm}}}](f_k) = A_k\sqrt{N}$ above the noise level. A Taylor window is then used to push the sidelobes from the ringing effects that will occur for incoherent signals, to below the noise level by choosing the signal to lobe ratio (SLR) to $\text{SLR} = \max_{\text{k}}(\text{A}_{\text{k}})\sqrt{\text{N}}$. This is assuming that the $\max(\text{S}_{\text{mbc}}) > \max(\text{S}_{\text{target}})$.

3.2 Processing

In the *Theory* chapter, we mentioned the MTI filter which can be used to reduce the effect of the main beam noise. However since the MTI filter is not made to be implemented on a signal with missing data even more samples might need to be sacrificed to implement this filter, since $x_{k+1} - x_k$ can not be performed around the missing data samples. Due to this a strong main beam clutter signal in relation to the target must be introduced to the model and first after the algorithms have been used can a MTI filter be applied to the recovered signal to eventually reduce the

noise from the main beam clutter. This has not been done in the *Result* chapter and instead we examine the returned data from the algorithms so the filtering does not affect and complicate the examination of the performance of the algorithms.

3.3 Measuring Performance

In equation (3.1), we introduced a target signal, a main beam clutter signal and a noise signal and we want to examine the effect on the outgoing signal from the algorithm by changing the relative strength between the target and the MBC as well as change the duty factor of the disturbance.

Since we are creating the signal we know where the main beam clutter and the target signal should be which is shown in Figure 3.2. The different cases we want to evaluate all contain a main beam clutter with the strength of $40dB$ per pulse and a 0 frequency (the main beam frequency can be shifted to this frequency as explained in the section *Example Scenario* in chapter 2, a target signal with strength varying from $-10dB$ to $30dB$ and a frequency of 138 (which is a frequency far away from the S_{mbc} but still not in the middle of the sample), Gaussian noise with the parameters $N_0 = 1$, $\sigma = 1$, and $\mu = 0$, and a duty factor varying from 0 to 0.4. This will be done for both the periodic disturbances and the random disturbances.

In the returning signal from the algorithms one can measure how the different areas in Figure 3.2 vary depending on the variables and what algorithm was used. The measurements of interest were chosen to be:

1. Target strength.

2. Mean of the absolute value of the noise in the recovered signal - this will be the "noise level", see Equation (3.2).

3. Standard deviation of the absolute value of the noise in the recovered signal - this will be refered to as "standard deviation of the noise"

For the same set of variables the data was studied over a number of iterations to estimate the mean of the above measurements. Because of this we also chose to study the standard deviation of the noise level over the set of iterations at each duty factor and target strength combination. This was to see if the recovered noise level usually would appear close to the mean noise level and not just on average.

Another factor to take into account is the processing time of the algorithms. However our focus has mainly been to study if it is possible to have any use of these algorithms and thus the time aspect will not be studied thoroughly since we did not programmed the algorithms with the time aspect in mind and instead focused on code simplicity.

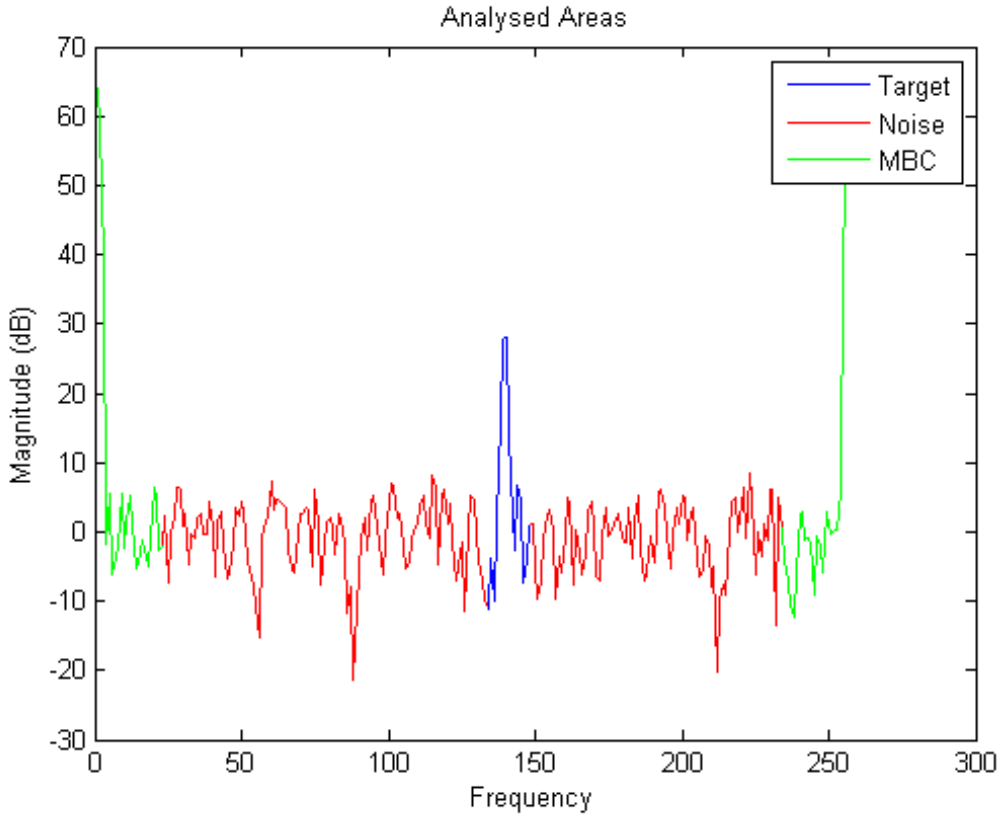

Figure 3.2: The figure describes the different areas that was analysed. It is here seen what was considered to be noise, target, and MBC. From the known location of the signals (MBC and target) a certain interval around this point was considered to be data points for that area. The rest was considered to be noise.

4

Results

In this section the performance of the missing data algorithms is examined. The first section examines the performance of the algorithms when they were influenced by random disturbance while the last section looks closer to the the algorithms performance when a periodic disturbance is applied.

4.1 Random Interference

The results in this section were gained by randomly removing a number of samples in accordance with the duty factor and then measuring the recovered target's strength, the mean noise level and the standard deviation of the noise in the returned signal. This was then redone 20 times and a mean value for the recovered target's strength, noise level and standard deviation was calculated and is presented in Figures 4.1-4.3.

By examining Figure 4.1, it is seen that the reconstructed target's strength correlated more with the original signal for the IAA and PD algorithm even for higher duty factors. This is not seen for CAMP and linear interpolation where the reconstructed target strength decreased with higher duty factor.

To be able to detect a small signal from a target, in a CFAR, a low noise level is desired and the reconstructed signal's noise level should preferably be as close to original signal's noise level as possible. In Figure 4.2, it can be seen that IAA and CAMP keep a low and constant noise level while the noise level is increased for the reconstructed signal by linear interpolation and PD with in regard to increased original target strength and duty factor. It should also be noted that some of the attributes of CAMP are to reduce the noise and compress the signal. The affect of this is seen in this Figure 4.2.

In Figure 4.3, the standard deviation of the noise can be seen. It is seen that linear interpolation and PD has a higher standard deviation for the noise for higher duty factors and target strengths, while IAA:s is not increasing as much. The standard deviation of the noise in CAMP is much lower than for the other algorithms. This is primarily due to that CAMP compresses frequencies and suppresses noise, which is illustrated in Figures 4.7 and 4.8.

The standard deviation for the 20 computed mean noise levels is seen in Figure 4.4. This is a measure of the variation of the created mean noise level from different random interference. If this deviation is low it means that independently of what scenario of missing data the algorithms have and the random change in the noise, the mean noise level will be about the same for a given duty factor and target strength. It is seen in Figure 4.4 that the variation is generally low for IAA but increases with higher target strengths as well as higher duty factor. PD has the highest fluctuation of the examined algorithms for the recovered noise levels and the fluctuations seems to be increasing with higher duty factor and target strength. The linear interpolation's variation of the reconstructed noise levels is generally low but is slightly increased for high target strength's with a low duty factor. But when removing more it becomes more stable in the sense of recovering the noise level to the same level. CAMP is good in generating the same noise level for the same target strength and duty factor.

Some more examples of the recovered frequency spectra is seen in Figures 4.5 - 4.8 and some of these will be referred to later in the *Discussion* and *Conclusion* chapter.

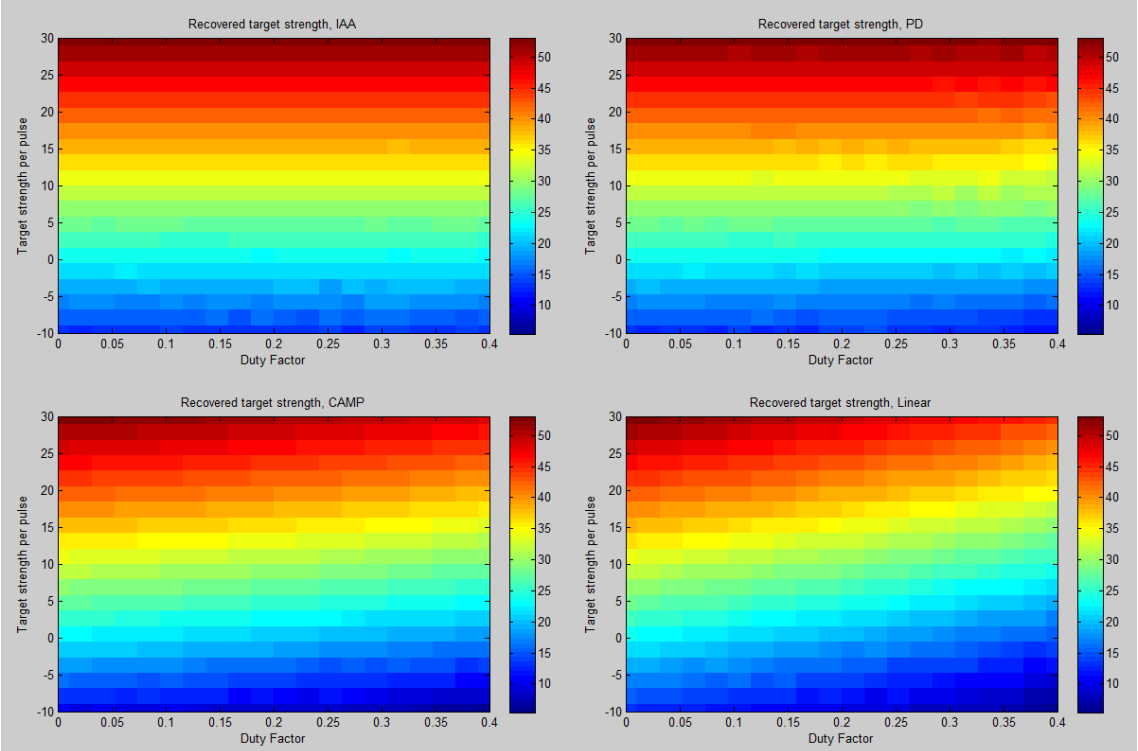

Figure 4.1: Visualising the mean target's strength in the recovered signal by varying the duty factor and the target's strength. Notice that the original reference is at duty factor 0 where no data points have been removed, the strength of the mean target's strength and the colorbar is given in decibel and the mean value was attained from 20 iterations.

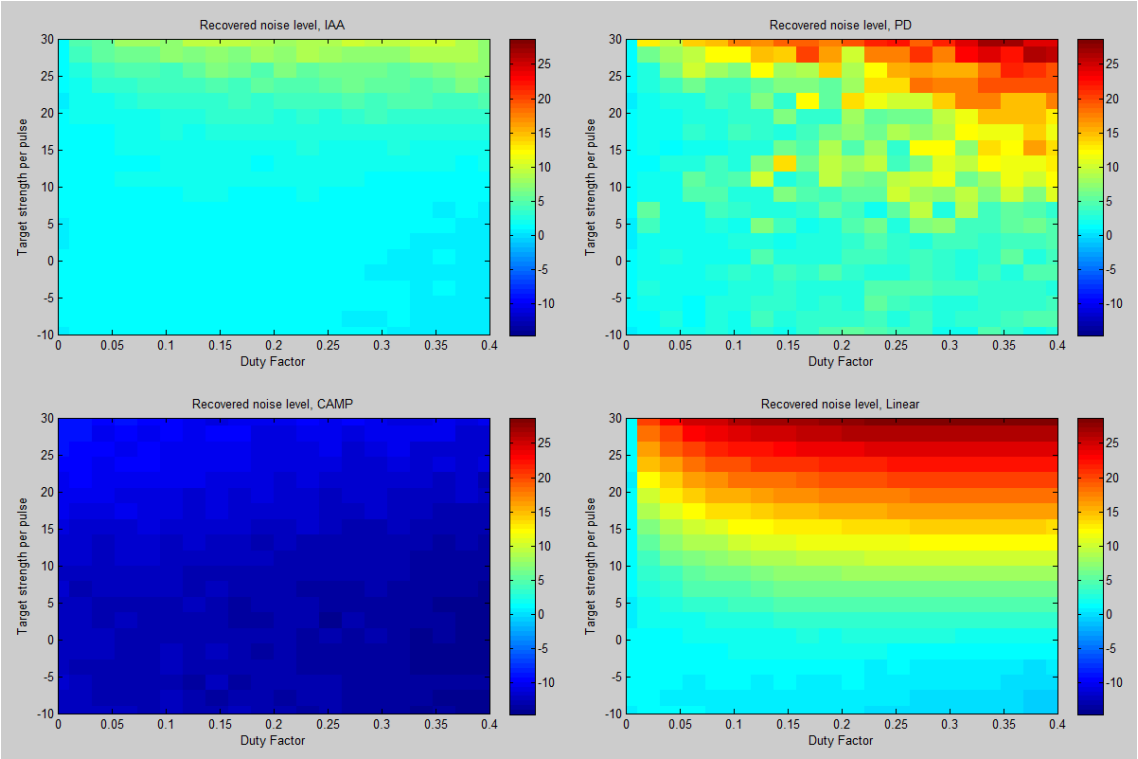

Figure 4.2: Visualising the mean noise level in the recovered signal by varying the duty factor and the target's strength. Notice that the original reference is at duty factor 0 where no data points have been removed, the strength of the mean noise level and the colorbar is given in decibel and the mean value was attained from 20 iterations.

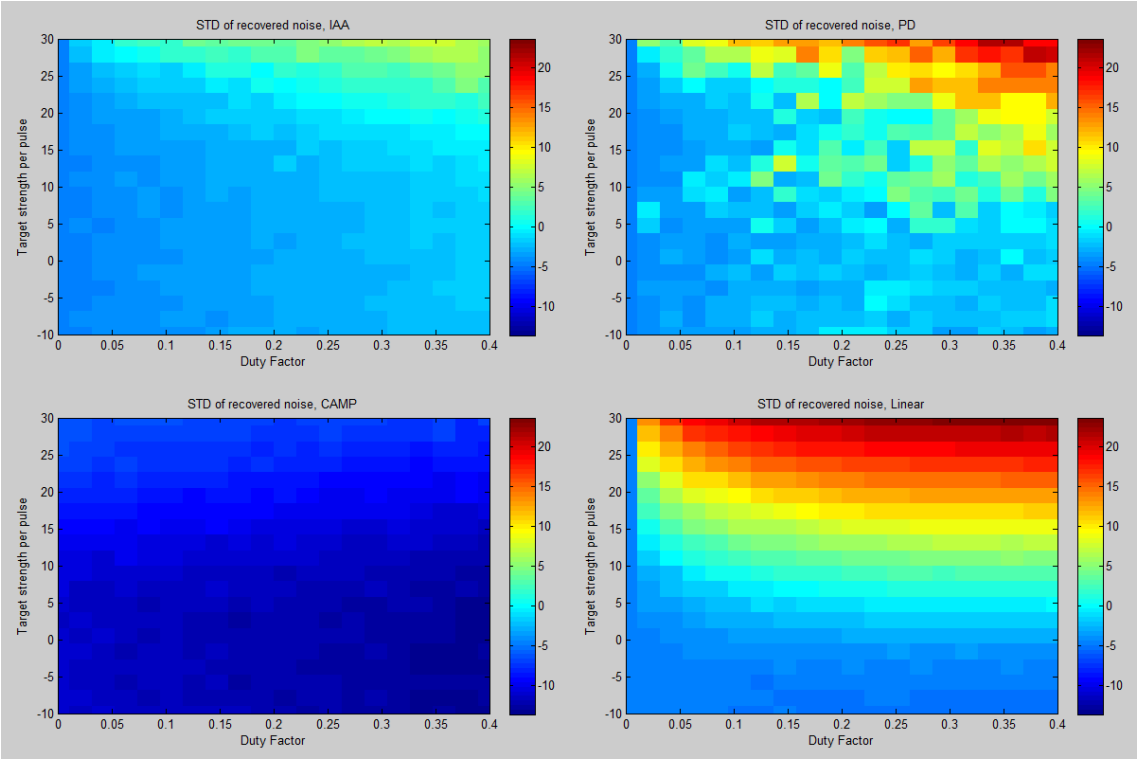

Figure 4.3: Visualising the mean standard deviation of the noise in the recovered signal by varying the duty factor and the target's strength. Notice that the original reference is at duty factor 0 where no data points have been removed, the strength of the mean standard deviation of the noise and the colorbar is given in decibel and the mean value was attained from 20 iterations.

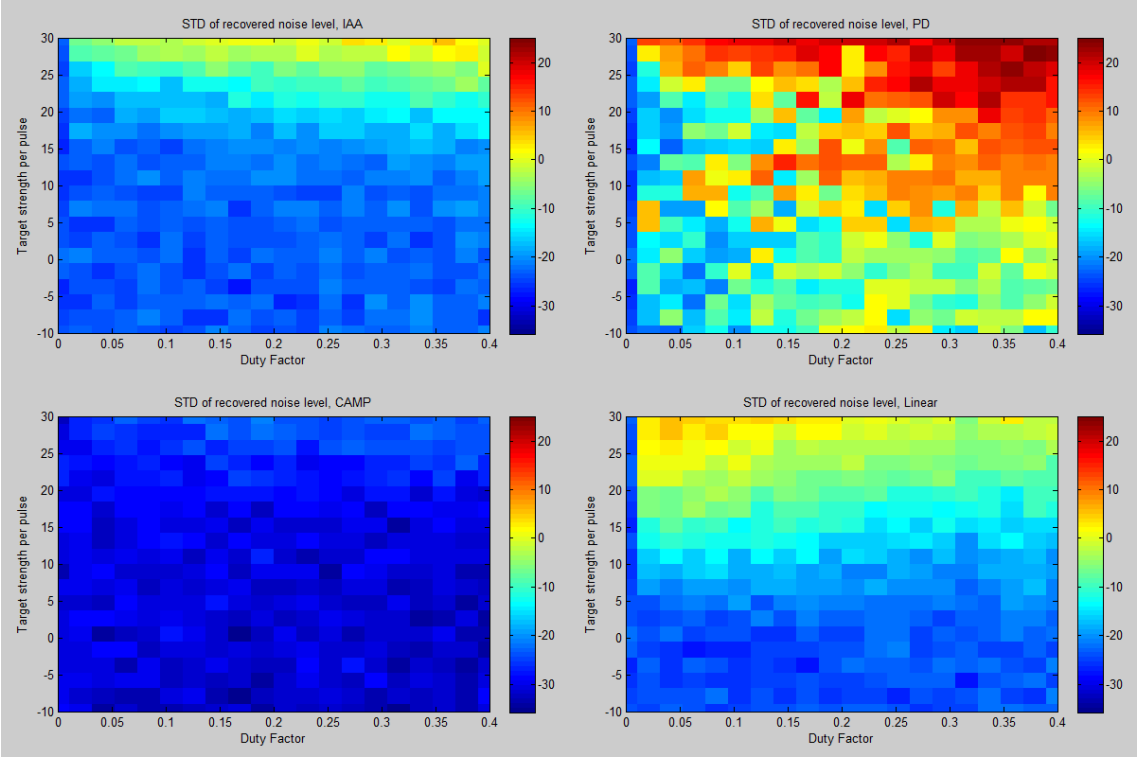

Figure 4.4: Visualising the mean standard deviation of recovered noise level over multiple iterations in the recovered signal by varying the duty factor and the target's strength. Notice that the original reference is at duty factor 0 where no data points have been removed, the strength of the mean standard deviation of recovered noise level over multiple iterations and the colorbar is given in decibel and the mean value was attained from 20 iterations.

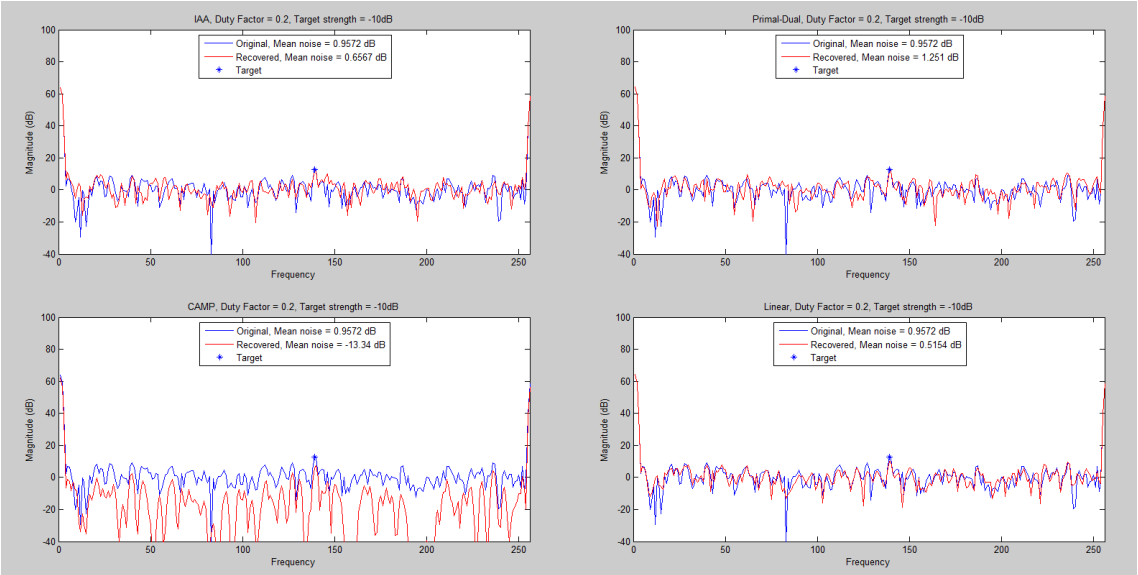

Figure 4.5: Comparing the recovered signal (red) and the original signal (blue) in the frequency spectrum for the four different algorithms. The blue star indicates the original strength of the target. Parameters used in this case were: target strength per pulse -10 dB and duty factor 0.2.

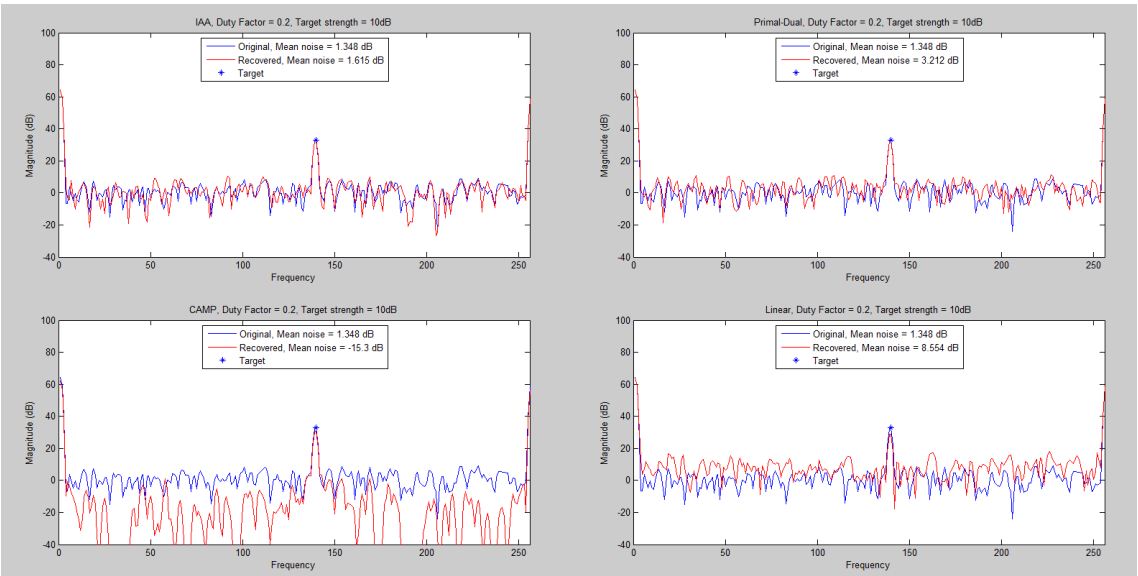

Figure 4.6: Comparing the recovered signal (red) and the original signal (blue) in the frequency spectrum for the four different algorithms. The blue star indicates the original strength of the target. Parameters used in this case were: target strength per pulse 10 dB and duty factor 0.2.

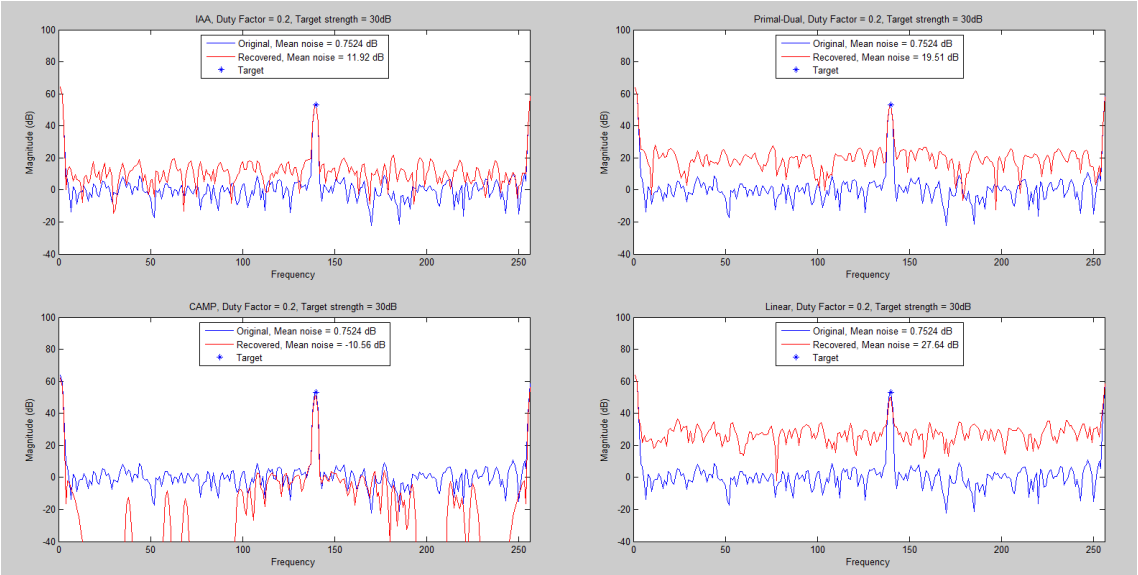

Figure 4.7: Comparing the recovered signal (red) and the original signal (blue) in the frequency spectrum for the four different algorithms. The blue star indicates the original strength of the target. Parameters used in this case were: target strength per pulse 30 dB and duty factor 0.2.

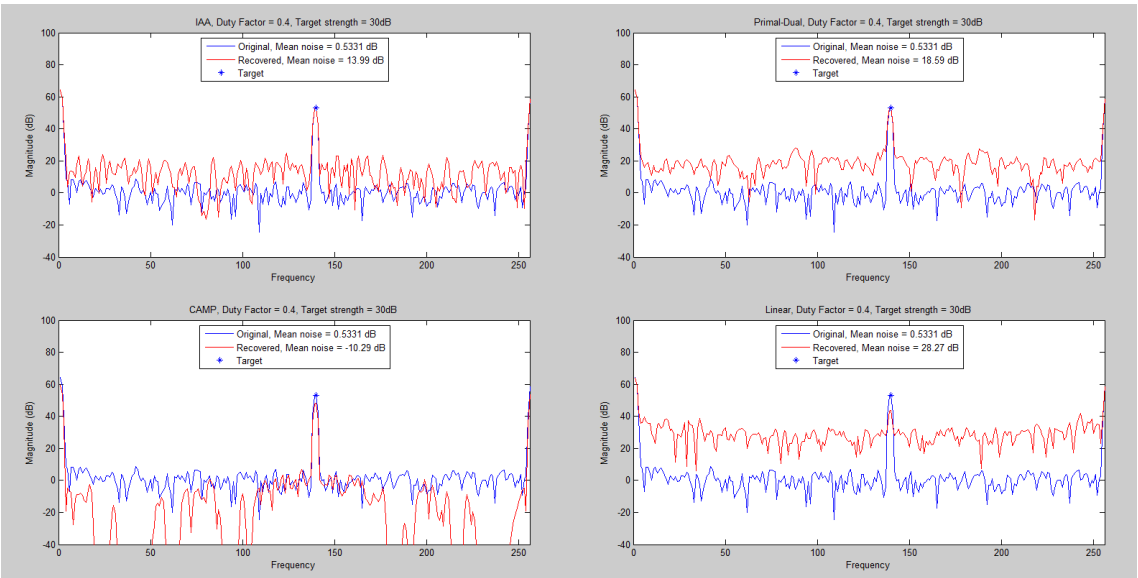

Figure 4.8: Comparing the recovered signal (red) and the original signal (blue) in the frequency spectrum for the four different algorithms. The blue star indicates the original strength of the target. Parameters used in this case were: target strength per pulse 30 dB and duty factor 0.4.

4.2 Periodic Interference

The results in this section were performed in a similar way to the previous with the exception that the missing data points were removed as a periodic band with 5 consecutive samples and not as random as in the previous section. The starting point of the first missing data band was chosen randomly in the range between the first and last index of the length of the disturbance band, which in this case was set to 5.

By varying the target's strength and the duty factor and measured the reconstructed target's strength, mean noise level, mean standard deviation of the noise and standard deviation of the 20 calculated noise levels was attained and can be seen in Figures 4.9 - 4.12[1].

The result of the reconstructed target's strength, in Figure 4.9, has many similarities with the result seen in Figure 4.1 which is the reconstructed target's strength from a random interference. However some differences are seen especially for CAMP and PD, there seems to be some discontinuity problem for CAMP around the duty factor of 0.3 and just below 0.4. The same is seen for PD at a duty factor around 0.25 and 0.35. This is due to ringing problems which occurs for these algorithms at these duty factors. An example of how a retrieved spectrum at these duty factors for PD and CAMP and the ringing effects is seen in Figures 4.14-4.17.

The mean noise level of the reconstructed signals is seen in Figure 4.10. In the figure we see that the noise level for linear interpolation increases with higher target strengths, and seem to be more independent of the duty factor than for the random disturbance. IAA's noise level is kept at a constant level for target strength's up to around 15 dB per pulse and then the noise level is slightly increased for higher target strengths. CAMP seem again to have some problem with discontinuities around the duty factor of 0.3 and just below 0.4 where the noise level is much higher than for lower frequencies. Otherwise it is seen that the noise level is reduced as expected. The noise level of PD is increased by ringing effects around 0.25 and 0.35 while the rest of the average mean noise levels resemble the levels which was gained from the random disturbance in the previous section in Figure 4.2.

In Figure 4.11, the mean standard deviation is seen. This deviation is low for IAA, in comparison with PD and IAA, for all duty factors and target strengths. We see that this deviation for linear interpolation is increased by a higher duty factor and target strength. This is due to ringing problems which emerge in the linear interpolation, and is illustrated in Figures 4.14 and 4.15. This deviation for CAMP is high for duty factors around 0.3 and above. This can again be related to the ringing effects which emerge for CAMP around these duty factors. The mean standard deviation of PD is seen to have a tendency to increase with higher duty factors and target strengths and have some problem with ringing around the already mentioned duty

[1]Notice that the first two duty factors give similar results. This is due to rounding off values when creating a row of missing data samples.

factors where ringing effects occur for PD.

In Figure 4.12, it is seen that linear interpolation and IAA are most consistent in reconstructing a similar noise level for a signal with the same duty factor and target strength. Some "discontinuities" can be seen for CAMP and PD and arise from ringing effects.

The difference between the the periodic interference and the random interference for CAMP and PD is probably due to ringing effects, and how this looks for CAMP can be seen in Figure 4.17. The ringing effects also emerge in the linear interpolation and PD and this can be seen in Figure 4.15.

Some more examples of how the recovered frequency spectra look are seen in Figures 4.13 and 4.14.

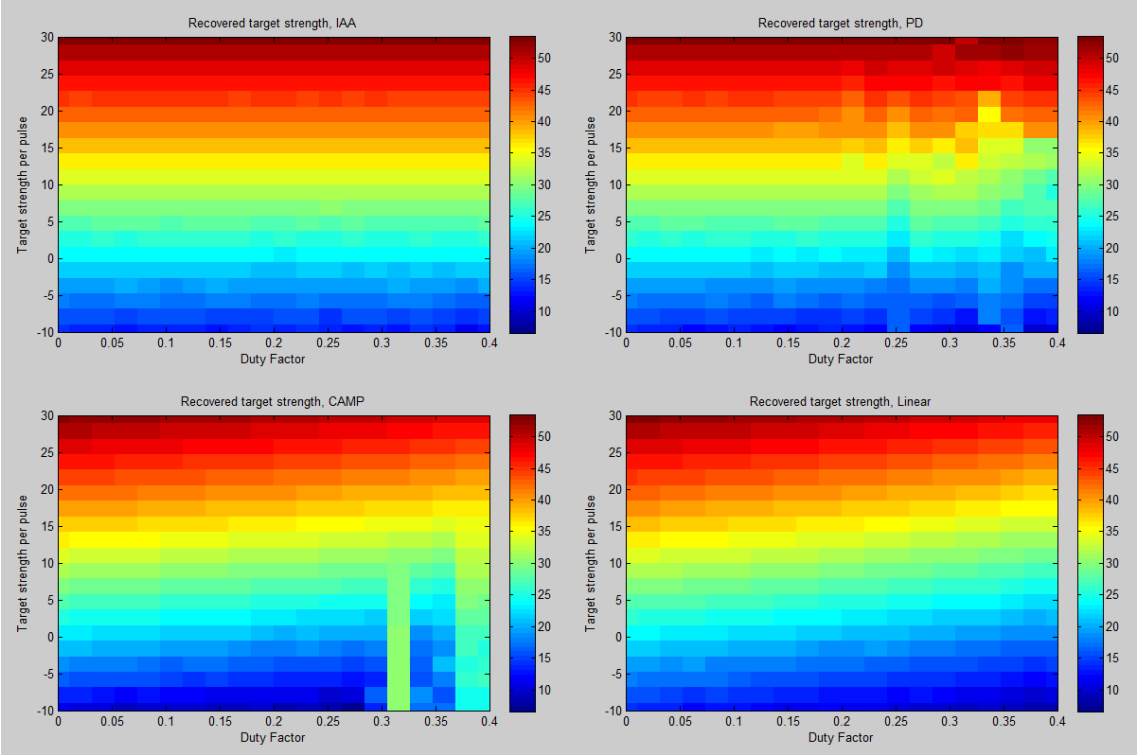

Figure 4.9: Visualising the mean target's strength in the recovered signal by varying the duty factor and the target's strength. Notice that the original reference is at duty factor 0 where no data points have been removed, the strength of the mean target's strength and the colorbar is given in decibel and the mean value was attained from 20 iterations.

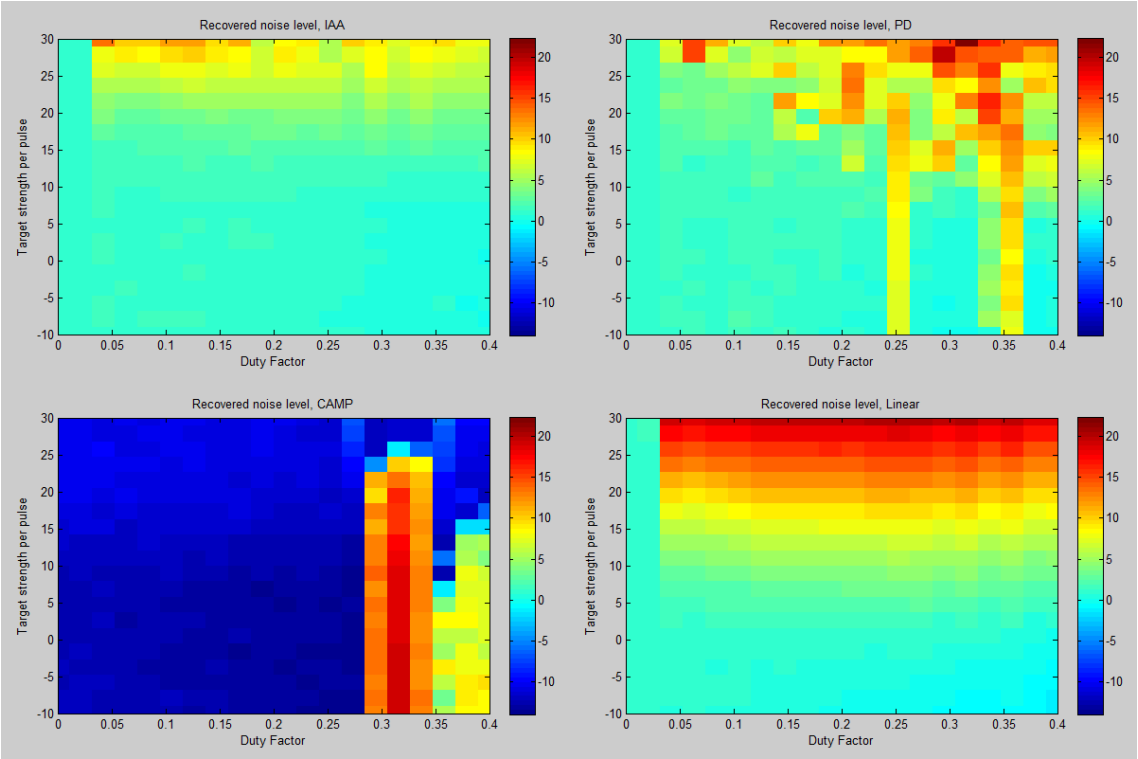

Figure 4.10: Visualising the mean noise level in the recovered signal by varying the duty factor and the target's strength. Notice that the original reference is at duty factor 0 where no data points have been removed, the strength of the mean noise level and the colorbar is given in decibel and the mean value was attained from 20 iterations.

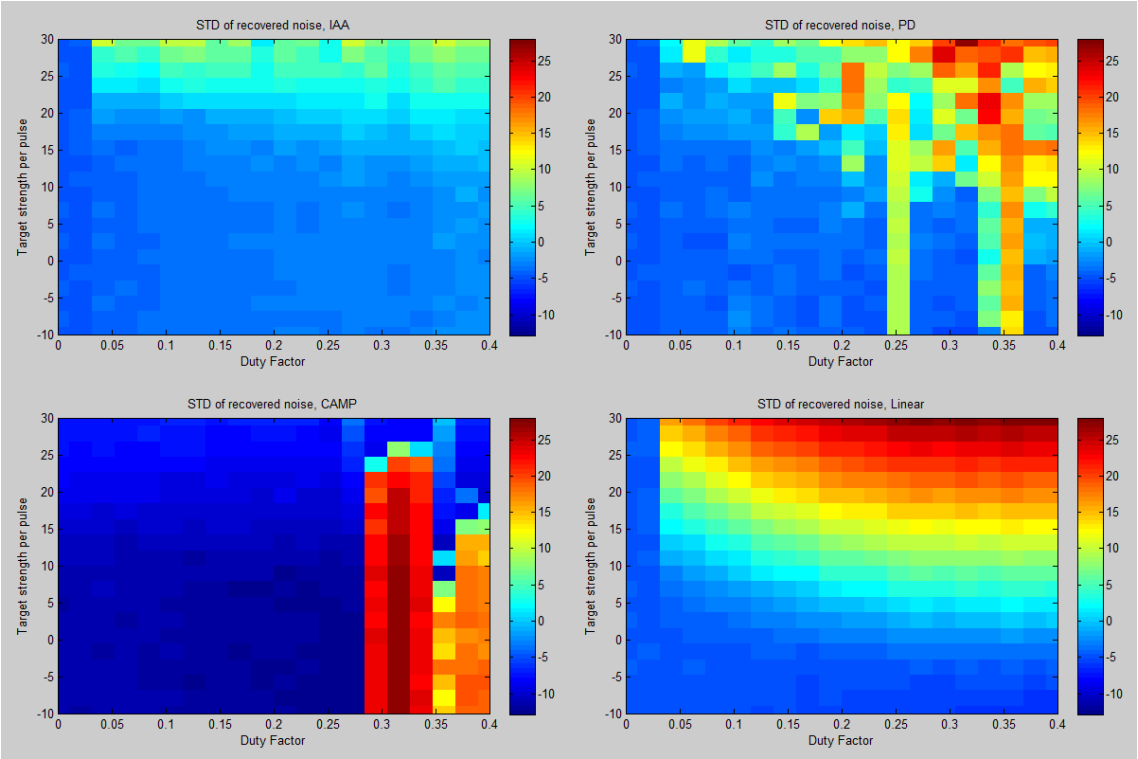

Figure 4.11: Visualising the mean standard deviation of the noise in the recovered signal by varying the duty factor and the target's strength. Notice that the original reference is at duty factor 0 where no data points have been removed, the strength of the mean standard deviation of the noise and the colorbar is given in decibel and the mean value was attained from 20 iterations.

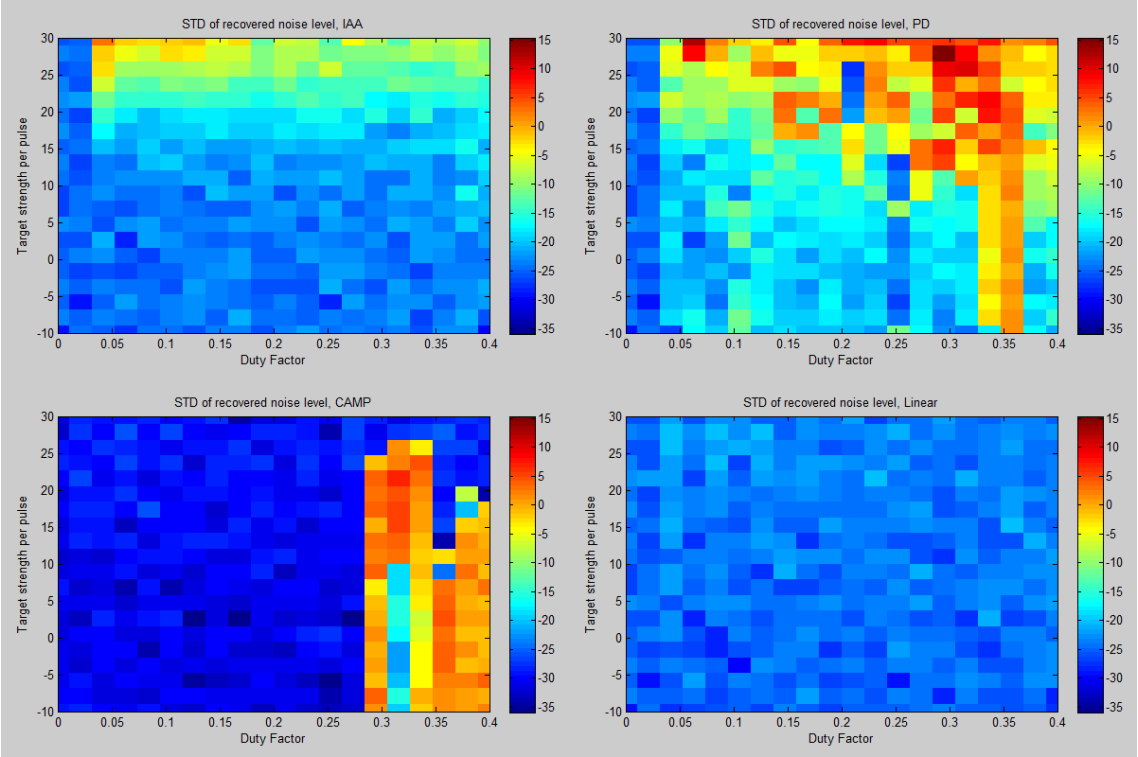

Figure 4.12: Visualising the mean standard deviation of recovered noise level over multiple iterations in the recovered signal by varying the duty factor and the target's strength. Notice that the original reference is at duty factor 0 where no data points have been removed, the strength of the mean standard deviation of recovered noise level over multiple iterations and the colorbar is given in decibel and the mean value was attained from 20 iterations.

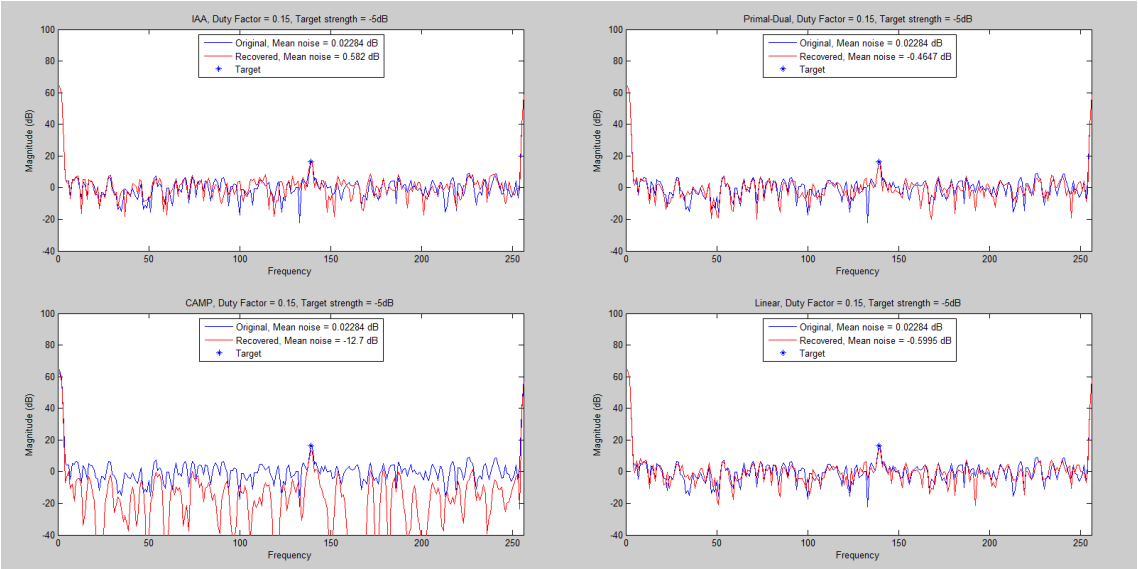

Figure 4.13: Comparing the recovered signal (red) and the original signal (blue) in the frequency spectrum for the four different algorithms. The blue star indicates the original strength of the target. Parameters used in this case were: target strength per pulse -5 dB and duty factor 0.15.

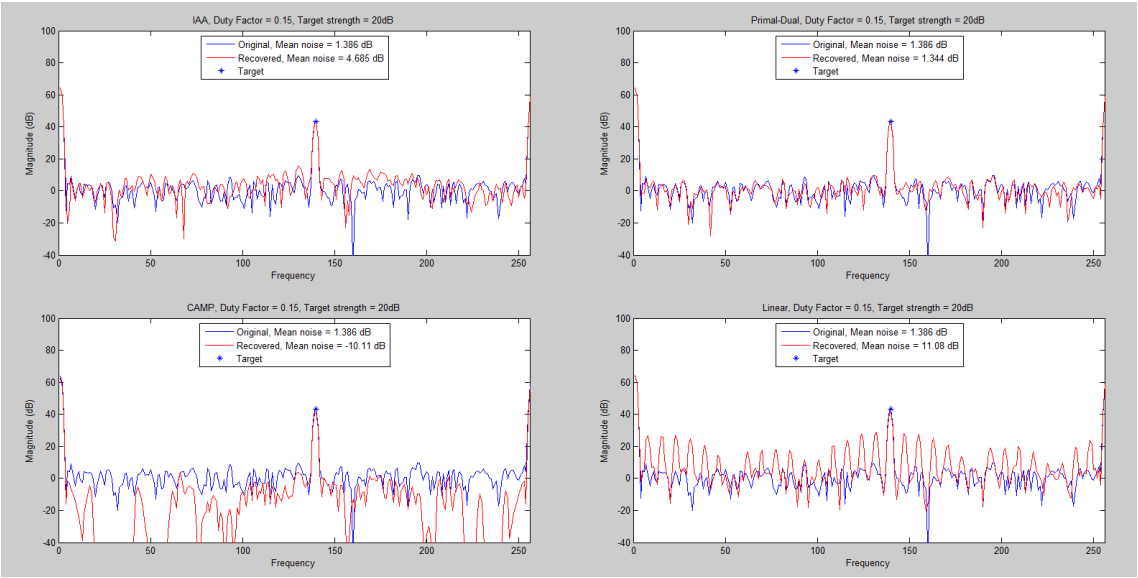

Figure 4.14: Comparing the recovered signal (red) and the original signal (blue) in the frequency spectrum for the four different algorithms. The blue star indicates the original strength of the target. Parameters used in this case were: target strength per pulse 20 dB and duty factor 0.15.

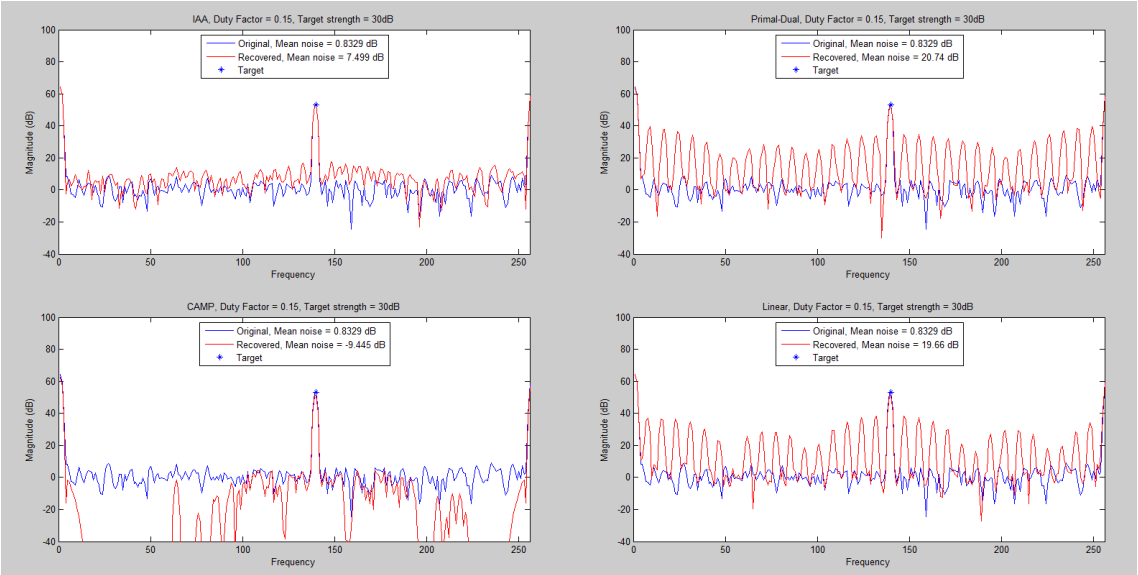

Figure 4.15: Comparing the recovered signal (red) and the original signal (blue) in the frequency spectrum for the four different algorithms. The blue star indicates the original strength of the target. Parameters used in this case were: target strength per pulse 30 dB and duty factor 0.15.

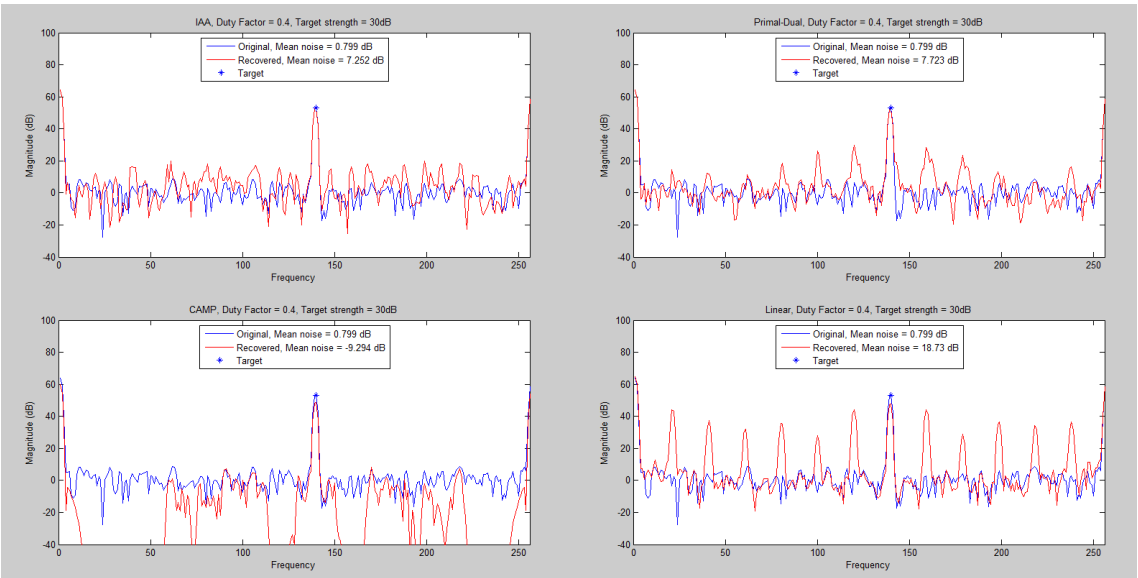

Figure 4.16: Comparing the recovered signal (red) and the original signal (blue) in the frequency spectrum for the four different algorithms. The blue star indicates the original strength of the target. Parameters used in this case were: target strength per pulse 30 dB and duty factor 0.4.

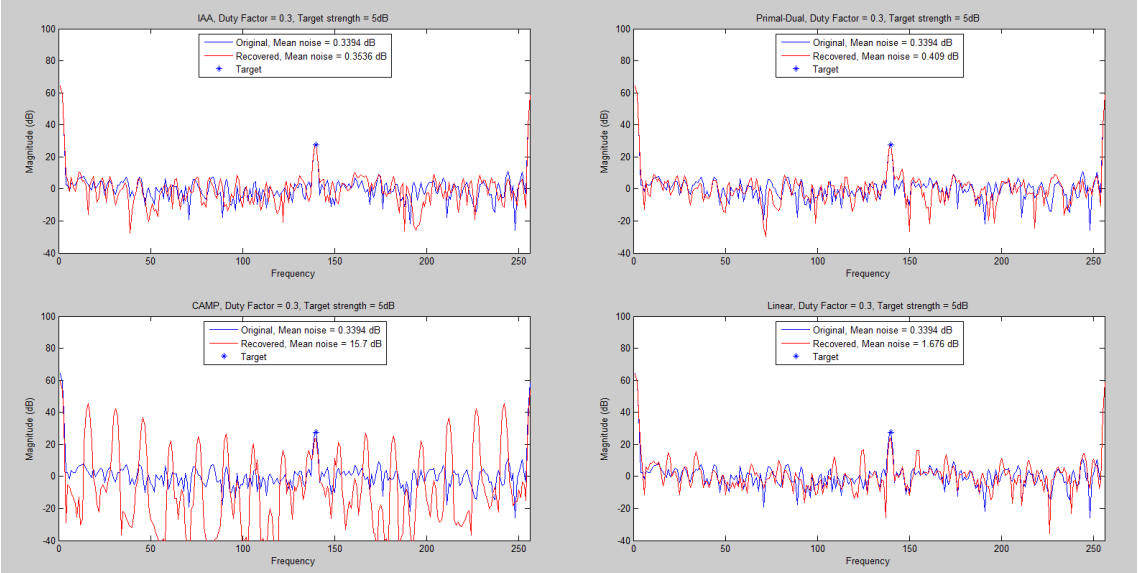

Figure 4.17: Comparing the recovered signal (red) and the original signal (blue) in the frequency spectrum for the four different algorithms. The blue star indicates the original strength of the target. Parameters used in this case were: target strength per pulse 5 dB and duty factor 0.3.

5

Discussion

The results shown in chapter 4 describe some of the characteristics of the algorithms' performance and how they work. The reason we chose to study these characteristics is because after the signal has been reconstructed by the algorithms it will be evaluated by a CFAR algorithm and from this information about the presence of a possible target can be gained. For a CFAR to work satisfactorily it is important that the target strength is not reduced by the algorithm and that the mean noise level and the standard deviation of the noise is low and reconstructed in a predictable way. However these results can also be deceptive. This is most obviously demonstrated in the mean noise level and the noise standard deviation in CAMP. CAMP is different from the other algorithms since it compresses some frequencies which reduces the noise. This might seem satisfying at first glance but it will result in a unpredictable CFAR detection since all of the non-compressed frequencies could be possible targets and can not be compared to neighbouring frequencies if these are compressed to zero. Otherwise we see that CAMP generally reconstructs a signal with slightly stronger target strength than the linear model (seen in Figure 4.1) while reconstructing a noise below the original signal's noise level and with lower standard deviation than the other algorithms (which is illustrated in Figures 4.2 and 4.3). If one had a way to estimate the expected noise level, CAMP could have been a useful algorithm for the problem which is encountered in this thesis.

Another disadvantage of CAMP is the characteristic ringing effects in the frequency spectrum which occur for periodic interference at specific duty factors, which can be seen in Figure 4.17. This ringing effect greatly reduces the prospect of detecting a target not just in the vicinity of the main beam clutter frequency but in the entire frequency spectrum.

We started this thesis with the assumption that the spectrum can be seen as sparse and due to this the compressive sensing algorithms PD and CAMP were introduced as well as IAA. We made this assumption since the number of frequency bins containing ground clutter and targets are generally low in comparison with the total number of frequency bins. Looking back at this assumption it may have been a misconception since the goal of the thesis was to reconstruct a signal which could be evaluated by a CFAR detection. If only the non zero amplitudes are used in the CFAR algorithm a new problem arises regarding how to set the guarding cells and training cells to give a suitable result for the detection algorithm.

The PD algorithm has some promising attributes such as recovering a strong target strength in the reconstructed spectrum independent of the duty factor for random disturbances, seen in Figure 4.1. This attribute was harder to see for periodic disturbances since ringing effects occurred at some duty factors, see Figure 4.9. However the noise level in the reconstructed signal by the PD algorithm varies more than the other examined algorithms and from our experience this algorithm is more noisy than the other algorithms which can be seen in Figures 4.4 and 4.12. This means that the noise level which is recovered will not always be recovered at the same level for the same duty factor and target strength but will vary due to the location of the disturbed samples and the randomness of the noise in the created signal. The uncertainty of the recovered noise level is a problem for a robust method of detecting targets. Furthermore PD also has some problems with ringing effects which can be seen in Figure 4.15.

IAA seems like one of the more promising reconstruction algorithms studied in this thesis since it is good at reconstructing the strength of the most dominating frequencies in the spectrum and keeping the noise level close to the same level as in the original signal, which is seen in Figures 4.1, 4.9, 4.2 and 4.10. Two worrying characteristic is that the standard deviation and the standard deviation of the noise level increases with higher target strengths' which should increase the probability of not being able to detect real targets, Figures 4.3, 4.11 4.4 and 4.12. However this effect is larger for the both linear interpolation and IAA also seems to be less prone to ringing effects which occurred due to the periodic missing data.

It is seen that the linear interpolation will increase the noise level (Figures 4.2 and 4.10) in regard to the duty factor. Also the standard deviation will increase for a higher duty factor and target strength (Figures 4.3 and 4.11) while the returned target strength will decrease for higher duty factors (Figures 4.1 and 4.9). However the algorithm seems to be robust. Robust in the sense that for a given value of the target strength and the duty factor. The noise level of the reconstructed signal will always be at a similar level, which can be seen in Figures 4.4 and 4.12. If it was not robust, the random phase of the target or the randomly distributed corrupted samples would be a factor in the reconstruction of the noise level. The linear interpolation is a good algorithm to use before the CFAR detection for random interference but will for high duty factors increase the mean noise level to a level where a weak target can not be detected which is illustrated in Figure 4.8. For periodic interference ringing effects will emerge for high duty factors which can be seen in Figures 4.14 and 4.15, and in the standard deviation of the recovered noise seen in Figure 4.11.

To be able to implement a missing data algorithm for a radar system the algorithm must be able to perform the operation fast. Time consumption is one aspect that has not been considered in this thesis or in the programming of the algorithm and must be evaluated before an algorithm can be used. Clearly the linear interpolation would be the fastest algorithm due to its simplicity.

Another interesting approach to the problem is to first use the missing data algo-

rithm to find the main beam clutter. The clutter frequency could then be removed from the original signal and a new operation of the missing data algorithm could be performed on the original data with the removed main beam clutter. However, this approach need more computations.

In future work it would be interesting to evaluate how the reconstructed signals perform in a CFAR algorithm or another detection algorithm is something that should be examined which would be more able to gain more information about the algorithms performance. This would tell us how many false alarms the algorithms give rise to and the probability of detecting the target for different type of disturbances.

6

Conclusions

In this thesis, we have examined whether it is possible to use missing data algorithms to reduce the effect of unwanted disturbances, which disturb the frequency spectrum retrieved by a pulse-Doppler radar. We have examined three different types of missing data algorithms. Two of these are types of compressive sensing named primal-dual interior point method (PD) and complex approximate message passing (CAMP), while the last examined missing data algorithm is iterative adaptive algorithm (IAA). For these algorithms to work we assume that the frequency spectrum is sparse which means that the time signal can be represented in a satisfying way by a few dominating bases in the Fourier basis. This assumption is made since usually only a few strong tones are seen in the the frequency spectrum for a specific range bin which arise due to background noise and possible targets in the search direction at a specific range. Finally a fourth algorithm was introduced, which is a simple linear interpolation which is used as a reference in the evaluation of the other missing data algorithms.

The evaluation of the algorithms was done on a synthetic signal which contains a strong tone from the main beam clutter, a target of varying strength and background noise. Then, samples were removed from the created signal in a random or periodic fashion resembling two different cases of disturbance and we used our algorithms to recreate the signal.

For the algorithms performance we conclude:

• IAA generally produce a signal with a good recovered target strength, a low noise level and a recreated noise level which is about the same as for an incoming signal with a specific duty factor and target strength. The variation of the noise is increased for higher duty factors and target strengths' and could make a detection harder in the recovered frequency spectrum. It is also the algorithm which is least prone to experience problems with ringing for a periodic disturbance.

• Linear interpolation is an algorithm which is simple and easy to understand. It is robust in the way that, for a specific duty factor and target strength, the reconstructed noise level remains consistent throughout the iterations. The noise level is increased in regard to the disturbance duty factor and the target strength in the incoming signal. It has problems with ringing for the periodic disturbance for

high duty factors and target strengths which these are also consistent throughout the iterations.

• CAMP is different in the sense that this algorithm compresses the noise. The target strength in the recovered signal is weaker compared to the target strength in the original signal and frequencies which are not MBC or target will usually be suppressed below the original noise level. This is seemingly good but in a CFAR detection one would need a way to estimate a noise level otherwise this is prone to produce false alarms as well.

• PD is good at reconstructing the target strength. The method has a large variation in the reconstructed mean noise levels and experiences problem with ringing for some specific duty factors of the periodic disturbance.

• An interesting continuation of this thesis would be to investigate how the algorithms perform in a CFAR detection in regard to creating false alarms and detecting the target for different type of disturbances.

Bibliography

[1] Maxwell, J. Clerk. "A dynamical theory of the electromagnetic field". *Philosophical Transactions of the Royal Society of London* 155 (1865): 459-512.

[2] Jiang, Qiuxi. "Network Radar Countermeasure Systems". *Network Radar Countermeasure Systems*. Springer Berlin Heidelberg, (2016): 243-272.

[3] Stimson, George W. *Introduction to airborne radar*. SciTech Publications, (1998).

[4] Rawat, Kumar Tarum. *Digital Signal Processing*. Oxford University Press, (2015).

[5] Milligan, Thomas A. *Modern Antenna Design* (2:nd ed.). John Wiley & Sons, (2005): 136.

[6] Folland, G.B. *Fourier Analysis and Its Applications*, American Mathematical Society, (1992).

[7] Candès, Emmanuel, Justin K. Romberg, and Terence Tao. "Stable signal recovery from incomplete and inaccurate measurements". *Communications on pure and applied mathematics* 59.8 (2006): 1207-1223.

[8] Ge, Dongdong, Xiaoye Jiang, and Yinyu Ye. "A note on the complexity of L_p minimization". *Mathematical programming* 129.2 (2011): 285-299.

[9] Boyd, Stephen,and Lieven Vandenberghe. *Convex Optimization*. Cambridge University Press, (2004).

[10] Candès, J. Emmanuel, and Justin K. Romberg. "l_1*-magic: Recovery of sparse signals via convex programming*". URL: `https://statweb.stanford.edu/~candes/l1magic/downloads/papers/BasisPursuit.pdf` 4 (2005): 14.

[11] Cheng, Hong. *Sparse representation, modeling and learning in visual recognition*. Springer, (2015).

[12] Eldar, Yonina C., and Gitta Kutyniok, eds. *Compressed sensing: theory and applications*. Cambridge University Press, (2012): 394-438.

[13] Maleki, Arian. "*Approximate message passing algorithms for compressed sensing*". Stanford University, (2010).

[14] Maleki, Arian, et al. "Asymptotic analysis of complex LASSO via complex approximate message passing (CAMP)". *IEEE Transactions on Information Theory* 59.7 (2013): 4290-4308.

[15] Stoica, Petre, Jian Li, and Jun Ling. "Missing data recovery via a nonparametric iterative adaptive approach". *IEEE Signal Processing Letters* 16.4 (2009): 241-244.